FINAL REPORT

Grant NGR 05-007-416, Supplement No. 3
March 25, 1975 - December 25, 1975

RESEARCHES ON INTERACTIONS OF SATELLITE-SPEED HELIUM ATOMS WITH ALUMINUM AND QUARTZ SURFACES

Prepared for

NASA Langley Research Center
Hampton, Virginia

by

Shih-Min Liu
Co-Principal Investigator
Assistant Research Engineer

and

Eldon L. Knuth
Principal Investigator
Professor

Molecular-Beam Laboratory
Energy and Kinetics Department
School of Engineering and Applied Science
University of California, Los Angeles
Los Angeles, California 90024

January 1976

I. SUMMARY

The present research program included three major experimental studies.

A. Spatial and Energy Distributions of Reflected Helium Atoms

Energy transfer in collisions of satellite-speed (7000 m/sec) helium atoms with a cleaned 6061-T6 satellite-type aluminum surface was investigated using the molecular-beam technique. Spatial and energy distributions of reflected helium atoms were measured and analyzed. Energy accommodation coefficients were then extracted from the measured distributions. These results are included in a separate report (see Appendix).

B. Gross Accommodation Coefficient inside an Aluminum Cavity

The gross accommodation coefficient for a satellite-speed (7000 m/sec) helium beam entering a 2-inch-diameter 6061-T6 aluminum spherical cavity was determined by measuring the exit velocity distribution of the leaving helium atoms using a metastable time-of-flight method. The mean velocity and energy reduced from the measured TOF spectrum are about 1535 m/sec and 0.054 eV respectively. These values correspond closely to the mean velocity and energy of a room-temperature effusive helium beam (i.e., $V_{\text{oven beam}} = 1550$ m/sec and $E_{\text{oven beam}} = 0.052$ eV at $T_{\text{oven}} = 300°K$). These results indicate that the 7000-m/sec satellite-speed helium atoms entering the cavity gain full accommodation with the room-temperature inner surface of the sphere through a large number of collisions before leaving the spherical cavity. As will be seen in Section III, these results validate the full-accommodation assumption frequently used in evaluating the mean velocity of gas atoms re-emitted from a satellite enclosure.

C. Arc-Heated Hydrogen Beams

The feasibility of producing a satellite-speed atomic hydrogen beam by arc-heating, for use in studies of interactions of satellite-surfaces

with hydrogen atoms under laboratory conditions, was investigated. It was found that a stable arc-heated molecular hydrogen beam can be obtained using Young's arc-heater, and that a partially dissociated hydrogen beam (i.e., a $H+H_2$ binary beam) can be produced by using a special high-temperature anode. However, a pure atomic hydrogen beam was not realized.

II. EXPERIMENTAL APPARATUS

The present experimental study was carried out in the UCLA Molecular-Beam Laboratory using the molecular beam system shown schematically in Figure II-1. The satellite-speed beams were generated by an arc-heated supersonic-beam source developed in this laboratory. The incident beam was collimated by a 0.10-inch-diameter orifice placed between the collimation chamber and the detection chamber; it was characterized by a multi-disk velocity filter located in the collimation chamber. Since the design and the operation of this selector have been discussed fully in [1], only a brief description will be provided here.

For a multi-disk selector, the nominal velocity u_o of the transmitted particles is determined by

$$\frac{L_o}{u_o} = \frac{\phi}{\omega} \tag{II-1}$$

i.e., the transit time for a molecule with speed u_o to travel the distance L_o between the first and the last disk equals the time required for the rotor with an angular velocity ω to rotate through the angle ϕ. Using a straight-slot approximation, one may calculate the nominal velocity of the transmitted molecules using

$$u_o = \frac{1722 \cdot f}{|\delta - \delta_o|} \quad \text{(m/sec)} \tag{II-2}$$

where f ($= \omega/2\pi$) is the rotor frequency measured in hz and $|\delta - \delta_o|$ is a linear displacement related to ϕ and measured in thousandths of an inch. (Cf. Ref. [1] for the derivation of Eq. (II-2) and the physical dimensions of the selector.)

---

[1] S. M. Liu, SEAS Report No. UCLA-ENG-7510, UCLA, 1975.

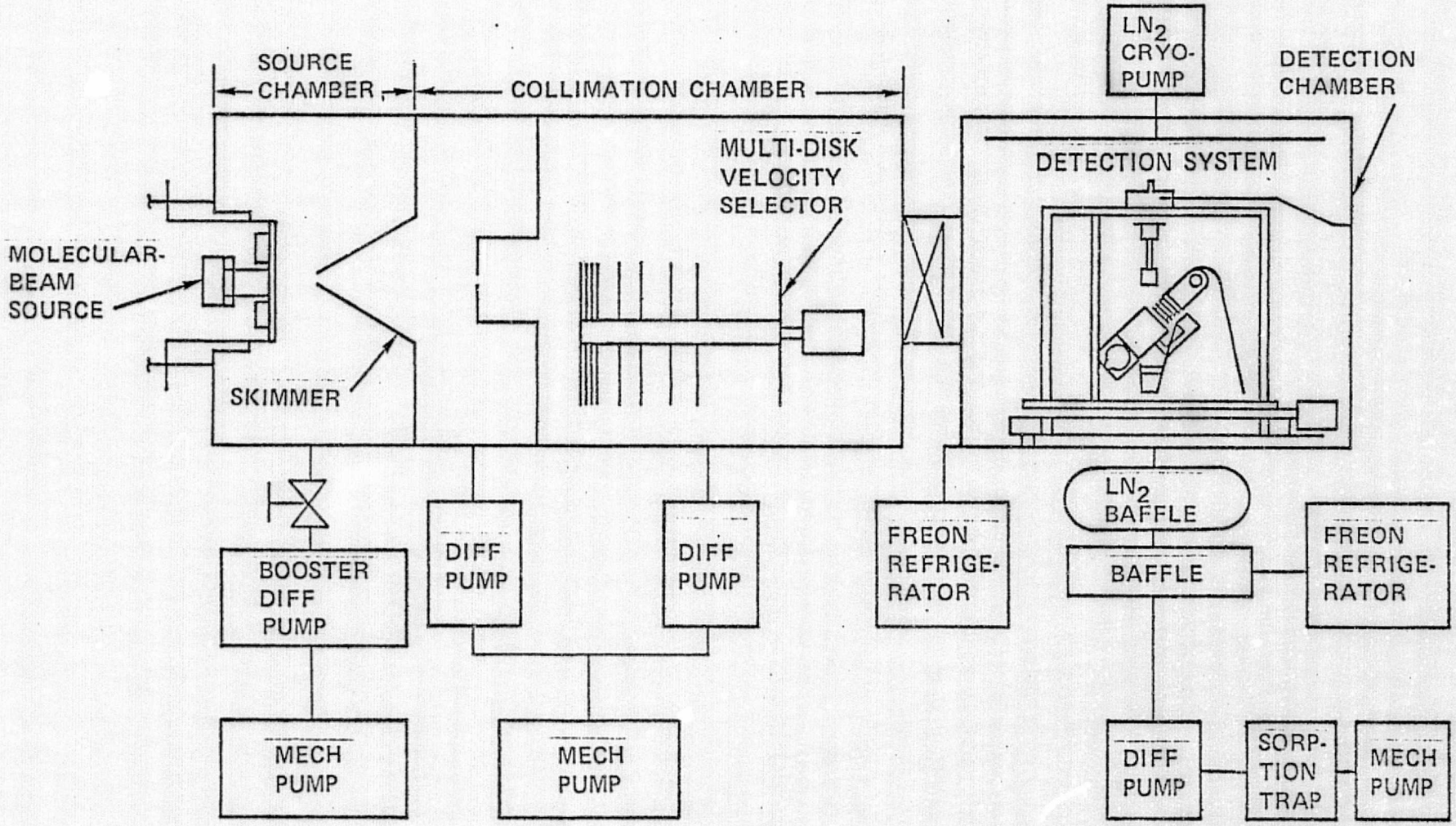

Figure II-1. Schematic Diagram of the Molecular Beam System.

Using this velocity selector, one may characterize the velocity distribution for a given incident beam by the transmitted beam signal measured by the mass spectrometer as a function of the rotation frequency of the selector at a preset displacement $|\delta-\delta_o|$. The mean energy of a molecular beam with a large hydrodynamic speed ratio can be approximated by

$$\bar{E}_i \cong 1/2\ m \cdot u_o^2$$

where m is the mass per molecule.

The nickle-plated detection chamber was pumped by a 10-inch oil-diffusion pump and a liquid-nitrogen cryopump. The background pressure in the detection chamber was 10^{-7} Torr (due mostly to nitrogen and oxygen) under normal operating conditions. Two detection systems were constructed during the course of this study to accommodate the first two experiments. A new mechanism for measuring the complete three-dimensional spatial and mean energy distributions of satellite-speed helium atoms reflected from satellite surfaces and a new time-of-flight detector for measuring the velocity distribution of helium atoms leaving a 2-inch aluminum sphere were built. These detection systems will be described in the following sections.

III. GROSS ACCOMMODATION COEFFICIENT INSIDE AN ALUMINUM CAVITY

An earth satellite using an on-board mass spectrometer for measuring the global density and composition patterns of the upper atmosphere often has an enclosing configuration as shown in Figure III-1. A major advantage of this design is that the density within the satellite is usually an order of magnitude higher than the ambient density, so that the sensitivity requirement of the on-board instrument can be relaxed. However, this configuration presents the problem of relating the measured density inside the satellite to the ambient density. It has been shown that the inside density and the outside density are related by

$$\frac{n_i}{n_e} = 4 \cdot G \frac{\bar{V}_{sat}}{\bar{V}_i} \left\{ \mathrm{erf}(S) \left[1 + \frac{1}{2S^2} \right] + \frac{e^{-S^2}}{S\sqrt{\pi}} \right\} \qquad \text{(III-1)}$$

where

n_i = density inside the satellite

n_e = density outside the satellite

$\bar{V}_{sat}$ = satellite velocity

$\bar{V}_i$ = exit velocity

S = speed ratio ($\equiv \bar{V}_{sat}/\bar{V}_{w,ex}$)

$\bar{V}_{w,ex}$ = mean random speed of ambient gas

G = geometrical factor (= effective entrance area/effective exit area).

However, in order to use Eq. III-1, one needs the value of the exit velocity $\bar{V}_i$. Often one assumes that particles have gained full accommodation with the inner surface before exiting from the satellite, so that one can determine $\bar{V}_i$ from the surface temperature T_s of the satellite. Possible deviations from this assumption might lead to significant errors. Hence, we describe here an experimental method for determining $\bar{V}_i$ under laboratory conditions.

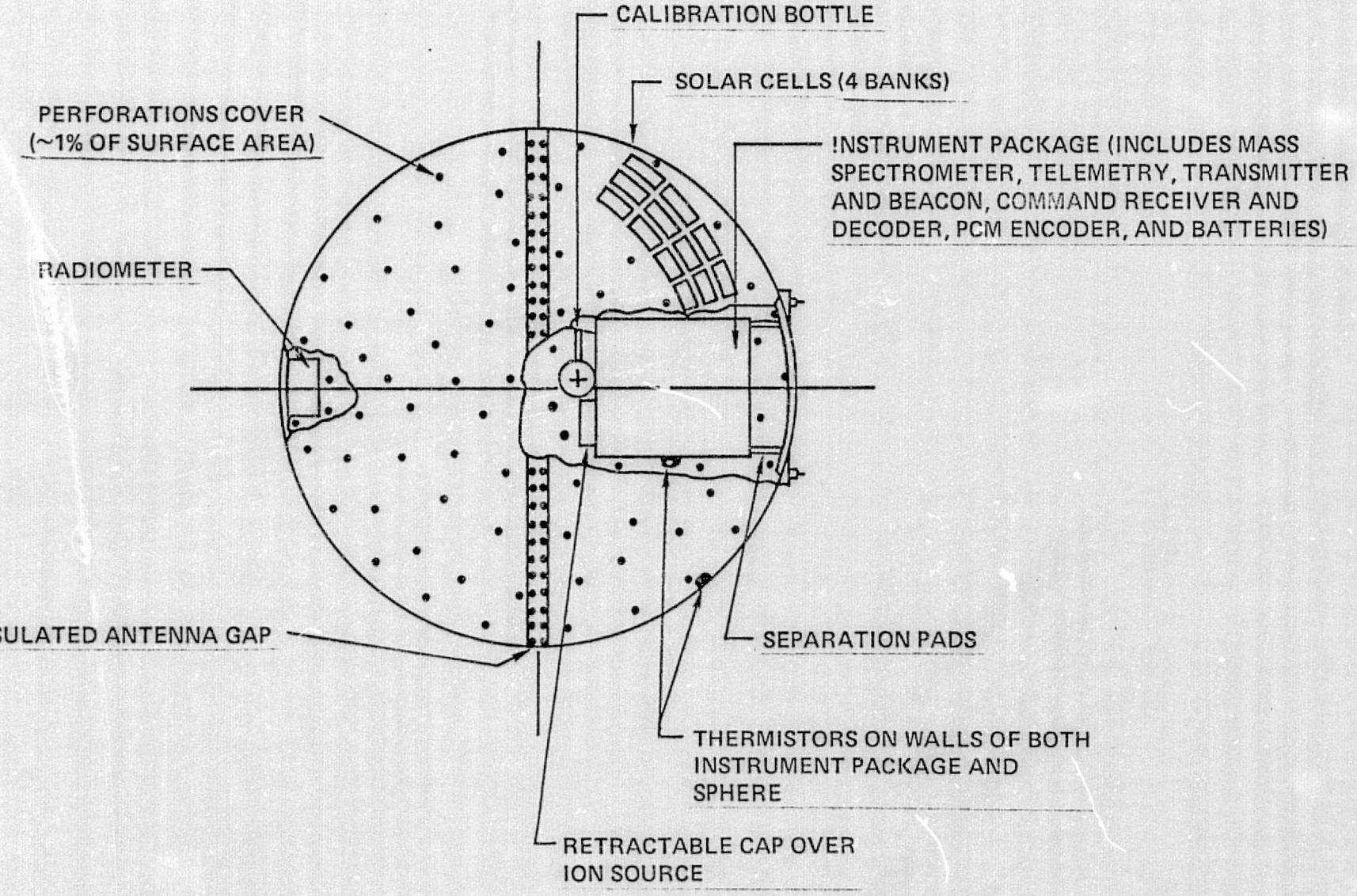

Figure III-1. Schematic Diagram of the NASA Dual-Air-Density-Explorer Drag Satellite.

The simplest and the most direct way to obtain the exit velocity is the spherical cavity method, which method simulates the actual conditions within the satellite. See Figure III-2. In this method, a beam with density n_b and velocity $\bar{V}_b$ enters the spherical cavity through an orifice with an effective area A_i. The exit velocity of the atoms leaving the cavity through a total area exit A_o can be determined using one of two alternative procedures:

A. Measure the exit velocity distribution of these atoms using the time-of-flight technique.

B. Measure the mean exit speed $\bar{V}_i$ from the measured steady state He density n_i inside the cavity using the simplified form of Eq.(III-1) for $S \gg 1$, i.e., using

$$\bar{V}_i = 4 \cdot \frac{A_i}{A_o} \cdot \frac{n_b}{n_i} \bar{V}_b \qquad \text{(III-2)}$$

Procedure A appears more direct compared to procedure B and avoids the necessity for careful measurements of n_b and n_i. Hence Procedure A was used in conjunction with a metastable TOF detector in this study.

The experimental setup is shown in Figures III-2 and III-3. A 7000-m/sec incident helium beam (5/16-in. diameter) entered the 2-in. dia. 6061-T6 aluminum spherical cavity through a 9/32-in. dia. hole. The TOF detector was positioned facing a second exit hole with the same diameter. The total exit area is about 1% of the spherical surface area, as in the NASA Dual Air Density Explorer Drag Satellites. Hence, the helium atoms entering the spherical cavity will experience, on the average, about 100 collisions with the inner satellite surface before escaping. A fraction of the helium atoms leaving the second exit hole were excited to metastable states (He*) by a pulsed electron beam. The pulse circuit for the exciter, as well as the data

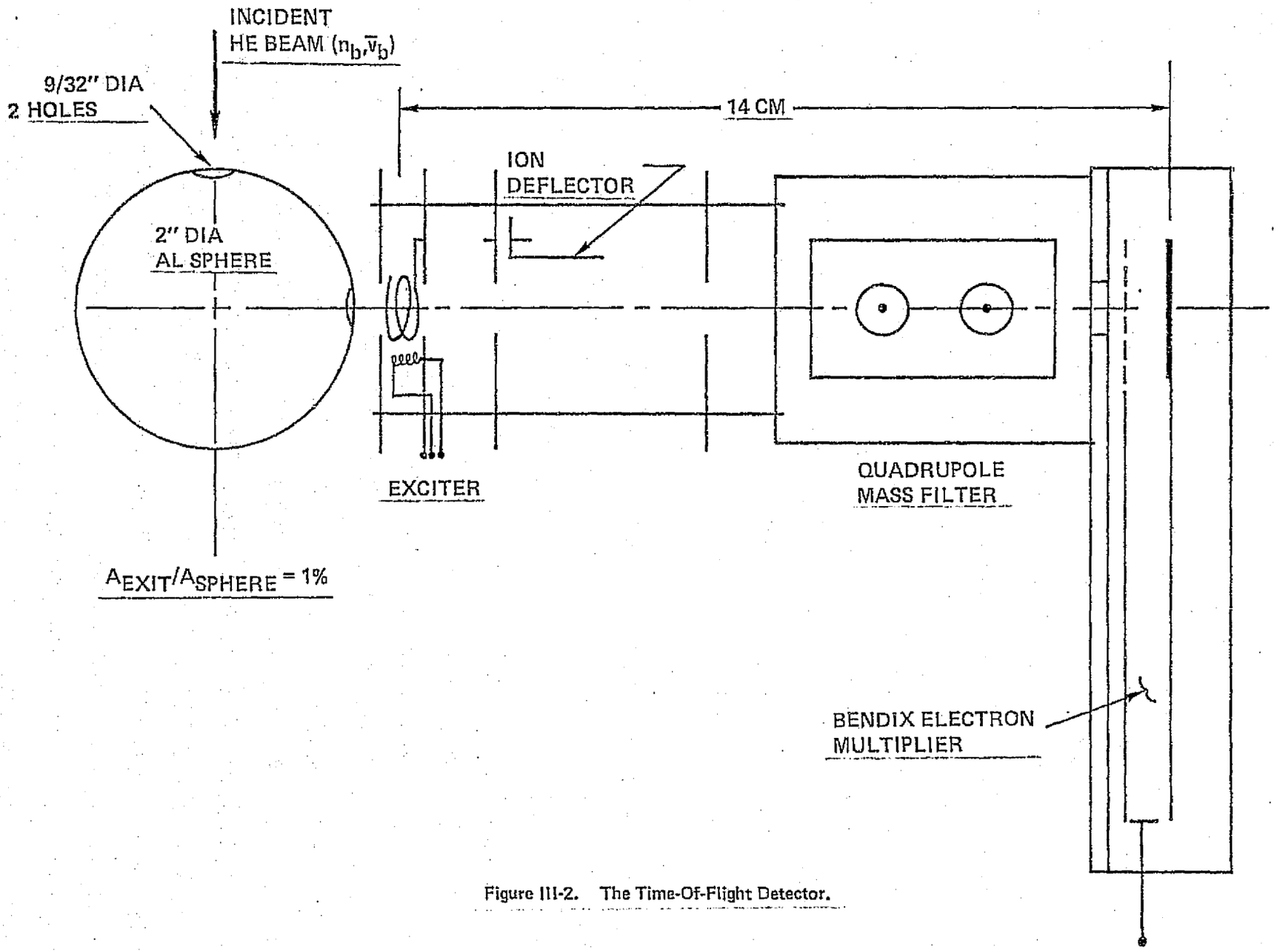

Figure III-2. The Time-Of-Flight Detector.

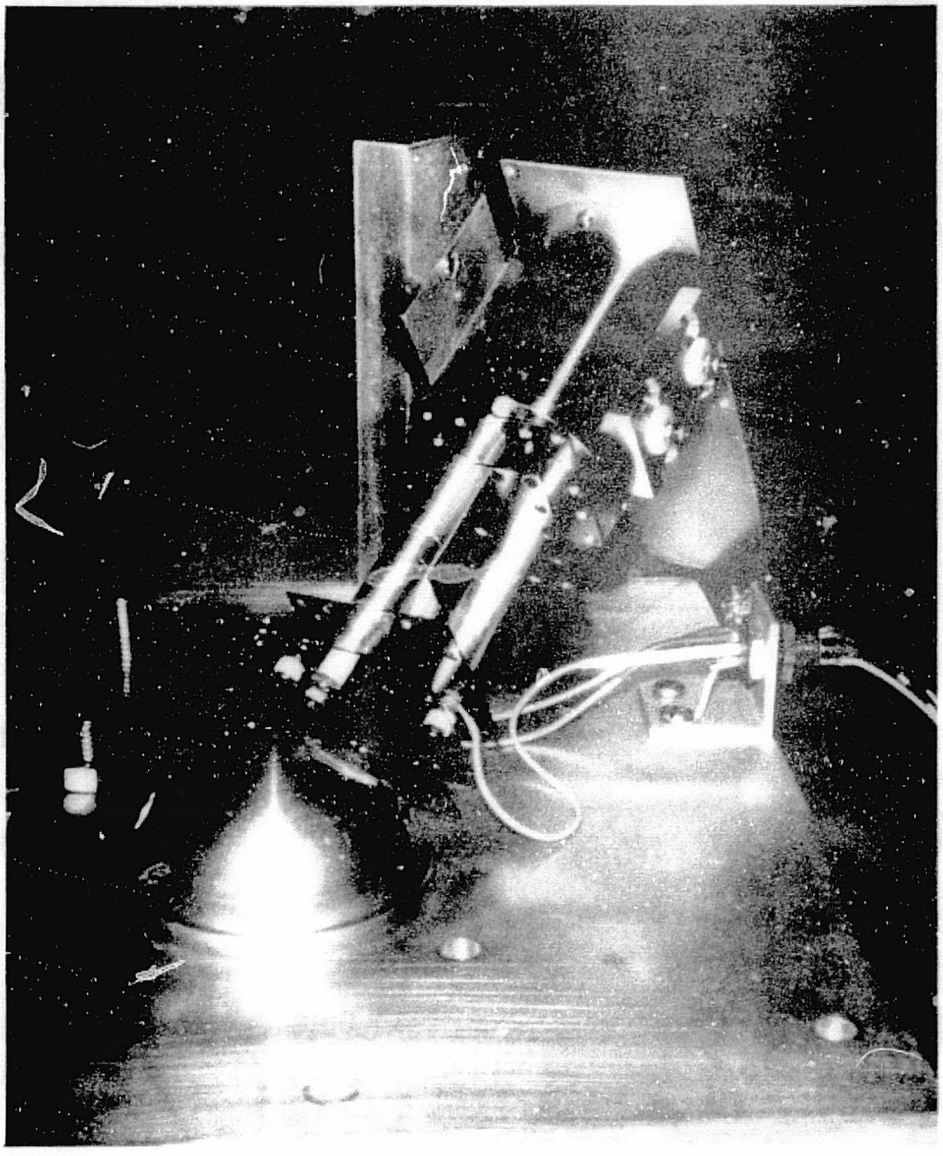

Figure III-3 Photograph of the Time-Of-Flight System

acquisition system, are shown in Figure III-4. Ions, a by-product of the excitation process, were eliminated by an electrostatic ion-deflector and a quadrupole mass filter. The He* TOF spectrum (i.e., the He* signal measured as a function of time for He* to travel a 14-cm flight path) was detected by a Bendix magnetic strip electron multiplier, processed by a PAR waveform eductor, and recorded on a photograph and/or X-Y chart.

Figure III-5 shows a photograph of a He* TOF spectrum and the applied excitation pulse displayed on a Tektronic dual-trace oscilloscope. The horizontal scale is 20 μs per cm. The zero-time reference is determined by the mid-point of the excitation pulse (i.e., t_o = (10/2-2) μs = 3 μs). Figure III-6 shows a plot of an X-Y recorder output of a He* TOF spectrum expressed as a function of true flight time (i.e., the flight time relative to t_o). Since the PAR waveform eductor has 100 memory channels, the horizontal scale is 2 μs per output channel. The mean velocity and energy of the helium atoms leaving the 2" aluminum sphere can be evaluated directly from these TOF data using the following formulas:

a. Mean Velocity:

$$\bar{V}_I = (\sum_i N_i(t) \cdot V_i)/(\sum_i N_i(t)) \qquad \text{(III-3)}$$

b. Mean Energy:

$$\bar{E} = (\sum_i N_i(t)(mv_i^2/2)/(\sum_i N_i(t)) \qquad \text{(III-4)}$$

where v_i = 14 cm/$(t-t_o)$ and i corresponds to the ith channel. The detail calculations are given in Table III-1. The mean velocity and the mean energy so determined are about 1535 m/sec and 0.054 eV respectively. Note that these values correspond closely to the mean velocity and energy of a room-temperature effusive helium beam (i.e., $\bar{E}_{oven} = 2kT_o$ = 0.052 eV and V_{oven} =

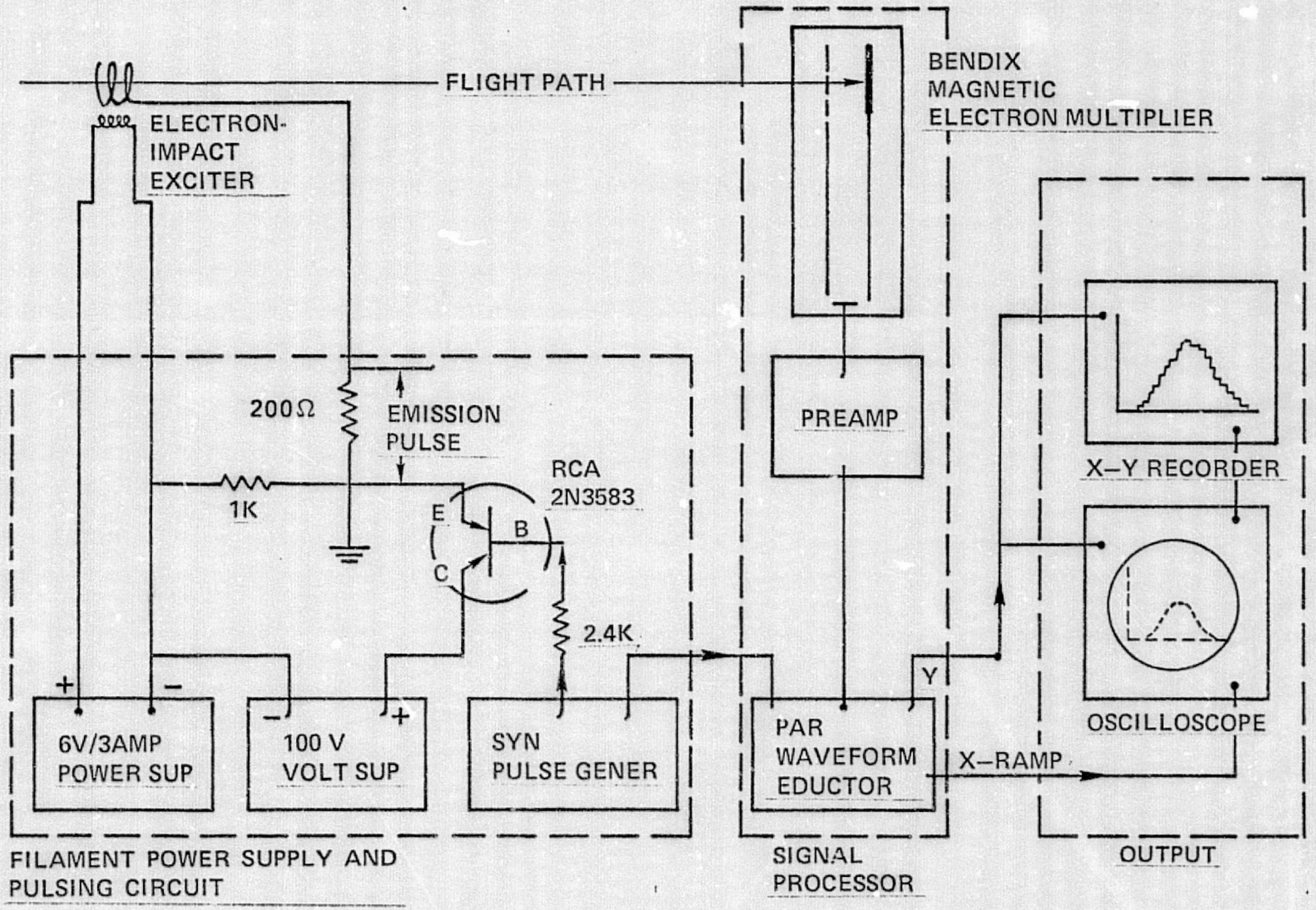

Figure III-4. Block Diagram of the Electronic System of the Metastable Time-Of-Flight Detector.

Sweep:
Duration: 200 μs
Delay(min.): 2 μs

Excitation Pulse:
Width: 10 μs

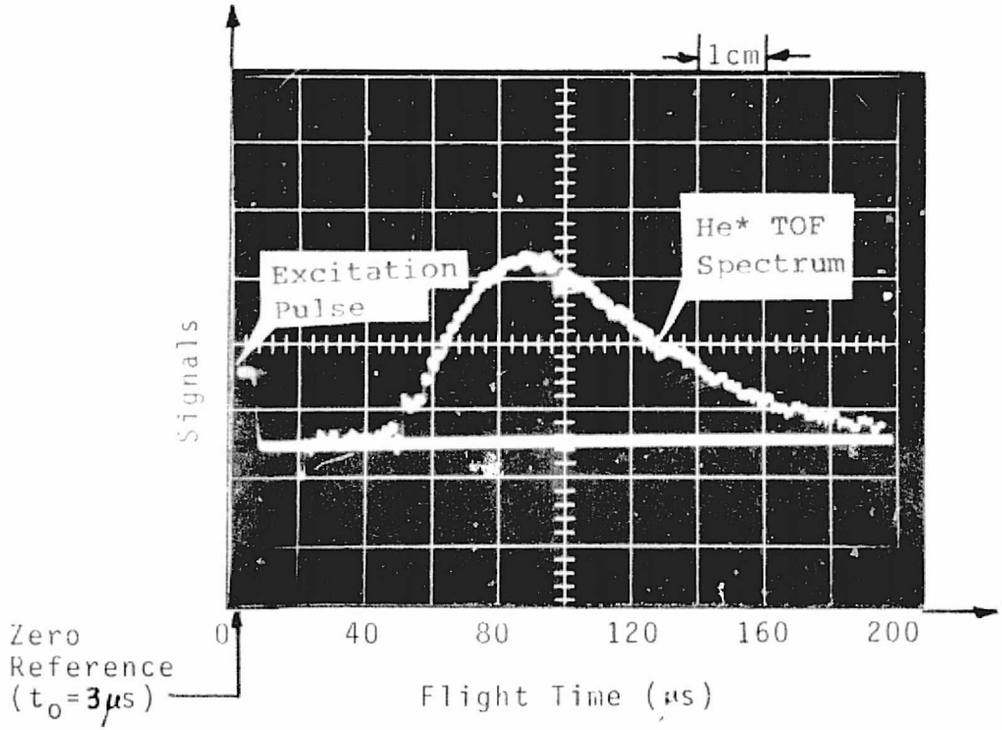

Figure III-5 Photograph of the He* Time-Of-Flight Spectrum

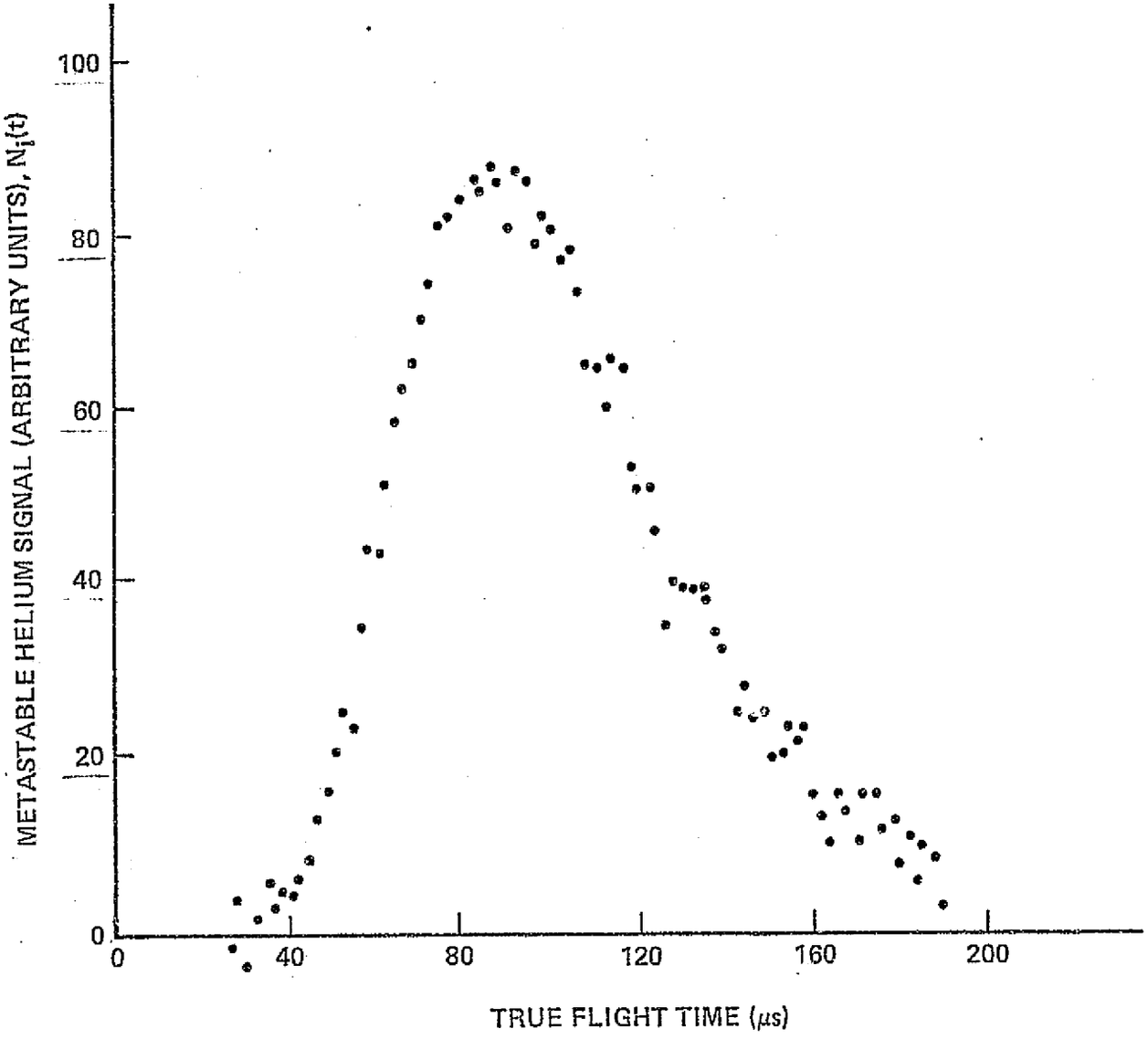

Figure III-6. Time-Of-Flight Spectrum of Helium Atoms Leaving a 2"- Dia Aluminum Cavity.

TABLE III-1

TOF Data of Helium Atoms Leaving a 2"-Dia. Aluminum Sphere

True Flight Time (μs)	Speed (m/sec)	Signal Height	Energy (eV)	Speed Distribution
$t-t_o$	v_i	$N_i(t)$	$mv_i^2/2$	$n_i(v)\%$
32	4375	2	.397	.0050
34	4118	6	.352	.0170
36	3889	3	.313	.0096
38	3684	5	.281	.0177
40	3500	4	.254	.0158
42	3333	6	.230	.0260
44	3182	8	.210	.0381
46	3043	13	.192	.0676
48	2917	16	.176	.0906
50	2800	20	.163	.1229
52	2692	25	.150	.1661
54	2593	23	.139	.1648
56	2500	34	.130	.2620
58	2414	44	.121	.3637
60	2333	43	.113	.3804
62	2258	51	.106	.4818
64	2188	59	.099	.5939
66	2121	62	.093	.6637
68	2059	65	.088	.7386
70	2000	70	.083	.8429
72	1944	74	.078	.9427
74	1892	81	.074	1.090
76	1842	82	.070	1.164
78	1795	84	.067	1.256
80	1750	86	.063	1.352
82	1707	86	.060	1.421
84	1666	85	.058	1.474
86	1628	88	.055	1.599
88	1591	86	.052	1.637
90	1556	81	.050	1.612
92	1522	87	.048	1.810
94	1489	86	.046	1.867
96	1458	79	.044	1.789
98	1429	82	.042	1.935
100	1400	81	.041	1.991
102	1373	77	.039	1.969
104	1346	78	.038	2.073
106	1321	73	.036	2.016
108	1296	65	.035	1.863
110	1273	65	.034	1.933

TABLE III-1 (CONT'D)

$t-t_o$	v_i	$N_i(t)$	$mv_i^2/2$	$n_i(v)\%$
112	1250	60	.032	1.850
114	1228	65	.031	2.076
116	1207	64	.030	2.116
118	1186	53	.029	1.814
120	1167	51	.028	1.805
122	1148	51	.027	1.865
124	1129	46	.026	1.738
126	1111	35	.026	1.366
128	1094	40	.025	1.611
130	1077	39	.024	1.620
132	1061	39	.023	1.670
134	1045	39	.023	1.721
136	1029	38	.022	1.727
138	1014	34	.021	1.591
140	1000	32	.021	1.541
142	986	25	.020	1.239
144	972	28	.020	1.427
146	959	25	.019	1.310
148	946	25	.019	1.346
150	933	20	.018	1.106
152	921	21	.018	1.192
154	909	24	.017	1.399
156	897	22	.017	1.316
158	886	23	.016	1.411
160	875	16	.016	1.007
162	864	13	.015	.8384
164	854	10	.015	.6610
166	843	16	.015	1.083
168	833	14	.014	.9710
170	824	10	.014	.7102
172	814	16	.014	1.163
174	805	16	.013	1.190
176	795	12	.013	.9135
178	787	13	.013	1.012
180	778	8	.013	.6370
182	769	11	.012	.8954
184	761	6	.012	.4992
186	753	10	.012	.8502
188	745	8	.012	.6949
190	737	4	.011	.3549

$\sum N_i(t) = 3247$

$\sum N_i(t).v_i / \sum N_i(t) = 1535$ m/sec

$\sum N_i(t).(1/2)mv_i^2 / \sum N_i(t) = 0.054$ (eV)

1550 m/sec at T_{oven} = 300°K). Hence it is concluded that the 7000-m/sec incident helium atoms entering the aluminum spherical cavity are fully accommodated with the room-temperature inner surface through a large number of collisions (about 100) before escaping from the cavity.

The velocity distribution can be obtained from the TOF spectrum using

$$n_i(v) = N_i(t)\cdot(t-t_o)^2/(\sum_i N_i(t)\cdot(t-t_o)^2)$$

The results are shown in the last column of Table III-1 and in Figure III-7.

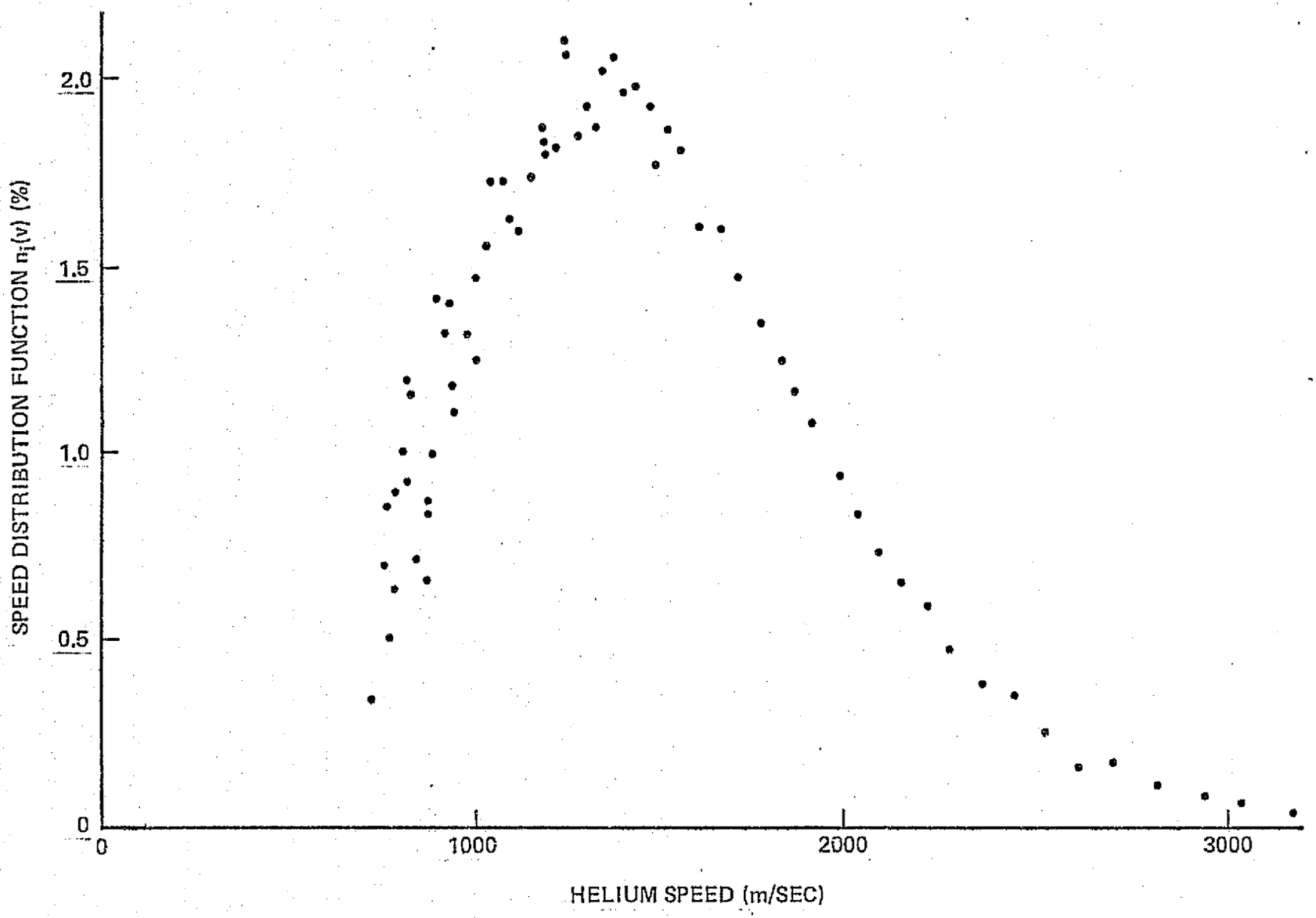

Figure III-7. Speed Distribution of Helium Atoms Leaving 2"-Dia Aluminum Cavity.

IV. ARC-HEATED HYDROGEN BEAMS

The feasibility of producing a satellite-speed hydrogen beam using arc-heating was investigated. More specifically, the design parameters, starting procedures, and operating parameters for obtaining a stable (and reproducible) satellite-speed hydrogen beam which would facilitate studies of interactions of hydrogen atoms with satellite-type surfaces were studied.

The arc-heater used in the scattering experiments to produce satellite-speed helium beams was used, with minor modifications, for this study. In particular, the nozzle diameter was increased from 0.050" to 0.100" to prevent melting of the copper anode due to excessive heat load. It was found that the most critical operating parameter is the hydrogen flow rate; the hydrogen arc is stable only within a narrow range of flow rate. If the flow rate is too high, the nozzle is eroded due to over heating. If the flow rate is too low, the arc becomes internal and damages internal components of the arc-heater.

It was found that a stable arc-heated hydrogen beam can be obtained using the following design parameters, starting procedure, and operating conditions:

A. Design Parameters

1. Nozzle: a threaded copper anode (replaceable) with a 0.100"-diameter orifice. Such a nozzle can be used repeatedly.
2. Anode-Cathode Gap: approx. 0.125"
3. Input Current to Magnetic Coil: approximately 10-12 amps.
   Field Strength: 600 Gauss

B. Starting Procedure and Operation Conditions

1. Light the argon arc with high argon flow rate. The power input is approximately 120 amps/15 volts.

2. Adjust P_{stg} to 50 torrs by lowering the argon flow. The input power might shift to 120 amps/20 volts.

3. Add hydrogen slowly until hydrogen flow rate reaches 10^{-3} mole/sec (22 std cc/sec). The stagnation pressure decreases first then increases beyond 50 torrs. It is necessary to use a good needle valve to control hydrogen flow.

4. Turn off argon flow slowly; keep input current at 130 amps. The input voltage will increase to approximately 30 volts. $(P_{stg})_{hot}$ = 35-37 torrs. (P_{cold} = 8.5 torrs.)

5. The input voltage will drop to 26-27 volts after a few minutes of running. The input current can be varied between 90 to 150 amps. The hydrogen flow rate can also be lowered to obtain various operating points.

Hydrogen beams produced using these techniques were characterized by the multi-disk velocity selector described in Section II. Typical measured velocity distributions are shown in Figure IV-1. The results show an excellent linear correlation between displacement $|\delta-\delta_o|$ and frequency f_p corresponding to the peak of the velocity distribution, as predicted by Eq. II-2. The approximate nominal velocities and corresponding beam energies are also shown in Figure IV-1.

Way et al. [2] reported some success in producing an atomic hydrogen beam with a flux on the order of 10^{15} atoms/cm^2-sec at a distance of 1 meter from the source. They also used Young's arc-heated beam-source design with minor modifications. Although they reported that energies of their atomic hydrogen beams ranged from 1.3 to 5.5 eV, the uncertainties in their measurements and the results for the molecular hydrogen beam obtained in this

---

[2] K. R. Way, et al., Int. Conf. Phys. Elect. Atomic Collisions, Seattle, Washington, July 1975.

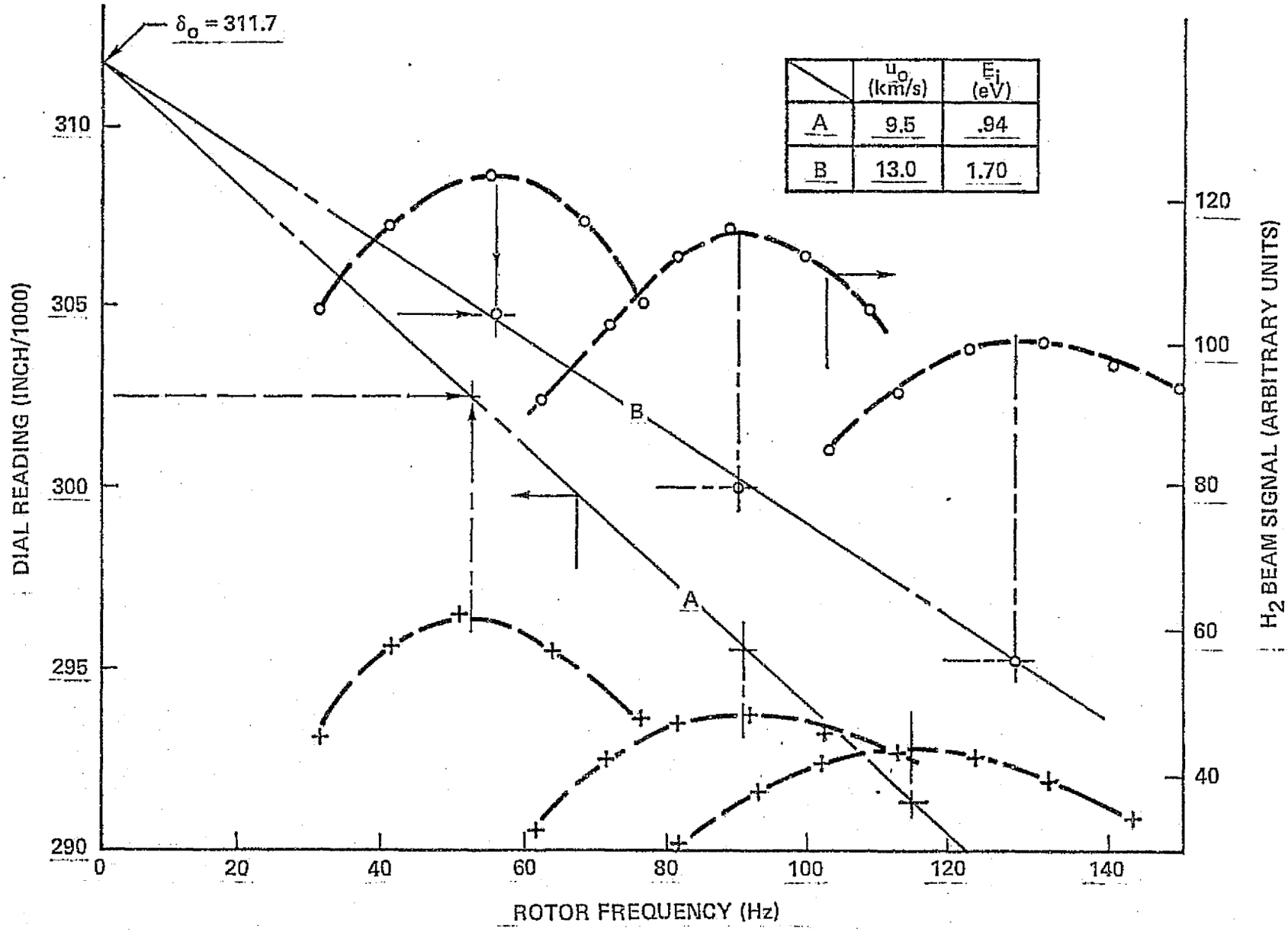

Figure IV-1. Velocity Distributions of H_2 Beams Characterized by the Multi-Disk Velocity Selector.

laboratory lead us to believe that the energy of the atomic hydrogen produced by this sourse is less than 2 eV. Winklemann [3] also produced a $H+H_2$ beam (with 30% dissociation) using Young's arc-heated beam-source design with a special W-Cu anode and a 0.050"-diameter orifice.

From the results obtained in this study and information provided by other investigators, the following conclusions regarding the production of arc-heated hydrogen beams are drawn: (1) a molecular hydrogen beam can be obtained using the design and procedures described at the beginning of this section; (2) a partially dissociated hydrogen beam (i.e. a $H+H_2$ binary beam) can be produced by using a special high-temperature anode which can endure a higher heat load and therefore allows the source to operate with a smaller nozzle orifice and a lower hydrogen flow rate; and (3) a pure atomic hydrogen beam would be difficult to obtain using arc heating.

---

[3] Private communication. He is at the Max-Planck Institut für Strömungsforschung, Göttingen.

APPENDIX

SPATIAL AND ENERGY DISTRIBUTIONS OF REFLECTED HELIUM ATOMS

FOREWORD

The researches described here were supported mainly by the National Aeronautics and Space Administration (under Grant NGR 05-007-416) and by the UCLA School of Engineering and Applied Science. These studies were part of a continuing program of researches in gas-surface interactions.

ABSTRACT

Energy transfer in collisions of satellite-speed (7000 m/sec) helium atoms with a cleaned 6061-T6 satellite-type aluminum surface was investigated using the molecular-beam technique. The amount of energy transferred was determined from the measured energy of the molecular-beam and the measured spatial and energy distributions of the reflected atoms.

Spatial distributions of helium atoms scattered from a 6061-T6 aluminum surface were measured again in this study, and show features similar to those presented in report UCLA-ENG-7546 [1]. The scattering pattern exhibits a prominent backscattering, probably due to the gross surface rougnesss and/or the relative lattice softness of the aluminum surface.

Energy distributions of reflected helium atoms from the same surface were measured for six different incidence angles. For each incidence angle, distributions were measured at approximately sixty scattering positions. At a given scattering position, the energy spectra of the reflected helium atoms and the background gas were obtained using the retarding-field energy analyzer. The mean reflected-beam energy and the differential energy accommodation coefficient ($(A.C.)_E(\theta_i,\theta_r,\phi)$) were then extracted from these spectra using a least-square fitting program. The measured $(A.C.)_E(\theta_i,\theta_r,\phi)$s show some fluctuations and a weak dependence on scattering angle, i.e., the accommodation decreases slowly as the scattering direction shifts toward the surface tangent.

The overall energy accommodation coefficient for a beam with a given incidence angle was then evaluated using the measured spatial density distributions and the mean reflected-beam energy distributions. Results show that the mean accommodation coefficient varies between 50% and 65%, dependent on the incidence angle.

TABLE OF CONTENTS

LIST OF FIGURES 27

LIST OF TABLES 28

LIST OF SYMBOLS 29

CHAPTER I - INTRODUCTION 30

CHAPTER II - EXPERIMENTAL APPARATUS AND PROCEDURES 31

CHAPTER III - RESULTS AND DISCUSSION 41

REFERENCES 59

APPENDIX 60

LIST OF FIGURES

II-1	Schematic Diagram of the Molecular-Beam System	32
II-2	Schematic Diagram of the Scattering System	33
II-3	Photograph of the Retarding-Field Energy Analyzer	34
II-4	Schematic Diagram of the Retarding-Field Energy Analyzer	35
II-5	Block Diagram of the Electronic System of the Retarding-Field Energy Analyzer	37
II-6	Complementary Beam-Surface Configurations of the Scattering System	40
III-1	Polar Plot of Scattered-Beam Density Distribution for 7000 m/sec Helium Beam Scattered from Cleaned 6061-T6 Aluminum Plate at 0° Incidence Angle	42
III-2	Polar Plot of Scattered-Beam Density Distribution for 7000 m/sec Helium Beam Scattered from Cleaned 6061-T6 Aluminum Plate at 15° Incidence Angle	43
III-3	Polar Plot of Scattered-Beam Density Distribution for 7000 m/sec Helium Beam Scattered from Cleaned 6061-T6 Aluminum Plate at 30° Incidence Angle	44
III-4	Polar Plot of Scattered-Beam Density Distribution for 7000 m/sec Helium Beam Scattered from Cleaned 6061-T6 Aluminum Plate at 45° Incidence Angle	45
III-5	Polar Plot of Scattered-Beam Density Distribution for 7000 m/sec Helium Beam Scattered from Cleaned 6061-T6 Aluminum Plate at 60° Incidence Angle	46
III-6	Polar Plot of Scattered-Beam Density Distribution for 7000 m/sec Helium Beam Scattered from Cleaned 6061-T6 Aluminum Plate at 75° Incidence Angle	47
III-7	Energy Spectra of the Reflected Helium Atoms Superimposed on the Background (Curve A) and the Thermal Background Helium Gas (Curve B)	49
III-8	Least-Square-Fitted Energy Spectra of the Reflected Helium Atoms and the Thermal-Background Helium Gas . . .	50
III-9	Overall Energy Accommodation Coefficient of a Satellite-Speed Helium Beam (1.02 eV) Scattered from a Cleaned 6061-T6 Aluminum Surface as a Function of the Incidence Angle	58

LIST OF TABLES

III-1 The Differential Energy Accommodation Coefficients and the Normalized Spatial Density Distribution for 7000 m/sec Helium Beam Scattered from Cleaned 6061-T6 Aluminum Plate at 0° Incidence Angle 51

III-2 The Differential Energy Accommodation Coefficients and the Normalized Spatial Density Distribution for 7000 m/sec Helium Beam Scattered from Cleaned 6061-T6 Aluminum Plate at 15° Incidence Angle 52

III-3 The Differential Energy Accommodation Coefficients and the Normalized Spatial Density Distribution for 7000 m/sec Helium Beam Scattered from Cleaned 6061-T6 Aluminum Plate at 30° Incidence Angle 53

III-4 The Differential Energy Accommodation Coefficients and the Normalized Spatial Density Distribution for 7000 m/sec Helium Beam Scattered from Cleaned 6061-T6 Aluminum Plate at 45° Incidence Angle 54

III-5 The Differential Energy Accommodation Coefficients and the Normalized Spatial Density Distribution for 7000 m/sec Helium Beam Scattered from Cleaned 6061-T6 Aluminum Plate at 60° Incidence Angle 55

III-6 The Differential Energy Accommodation Coefficients and the Normalized Spatial Density Distribution for 7000 m/sec Helium Beam Scattered from Cleaned 6061-T6 Aluminum Plate at 75° Incidence Angle 56

LIST OF SYMBOLS

$(A.C.)_E(\theta_i,\theta_r,\phi)$	differential energy accommodation coefficient at scattering position (θ_r,ϕ) for a beam with θ_i incidence angle
$\overline{(A.C.)_E(\theta_i)}$	overall energy accommodation coefficient for a beam with θ_i incidence angle
E_i	incident-beam energy
$E_r(\theta_i,\theta_r,\phi)$	energy of scattered helium atoms at scattering position (θ_r,ϕ) for a beam with θ_i incidence angle
$\tilde{E}_r$	energy of scattered helium atoms evaluated from its differential energy spectrum
$\tilde{E}_{ref}$	mean reference energy of thermal background gas evaluated from its differential energy spectrum
$f(E)$	differential energy distribution
$n_i(\theta_i,\theta_r,\phi)$	normalized spatial density-distribution function
$\hat{n}$	surface normal
$\hat{t}$	surface tangent
θ_i	incidence angle of helium beam measured from surface normal
θ_r	in-plane scattering angle measured from surface normal
ϕ	out-of-plane scattering angle measured from the plane of incidence
σ	standard deviation of the true reflected-beam energy spectrum from the least-square fitted function

CHAPTER I

INTRODUCTION

Basic knowledge concerning energy and momentum transfer between earth satellites and upper-atmospheric gases is essential for understanding the drag experienced by earth satellites (therefore for estimating the lifetime of an earth satellite and/or extracting the mean upper-atmosphere density from satellite drag data). For example, in predicting the aerodynamic drag of a satellite, one uses frequently a model in which the thermal accommodation between the ambient gas and the satellite surface is complete and the scattering distribution of reflected molecules follows the cosine law. However, possible deviations from this model might yield greatly different results.

These energy and momentum transfers can be investigated experimentally in the laboratory using an ultra-high vacuum system and the molecular-beam technique. The desired information can be extracted from the change in the beam properties during the surface collision if the states of both the incident and the scattered beam (spatial distribution and speed distribution) can be determined. Spatial distributions of satellite-speed helium beams scattered from satellite surfaces were obtained previously and summarized in report UCLA-ENG-7546. This report presents measured energy distributions of helium atoms reflected from 6061-T6 aluminum surfaces.

In Chapter II, the experimental apparatus and procedures are described briefly. Emphasis is given on the design and the operating procedure for the retarding-field energy analyzer. Experimental results are given and discussed in Chapter III. A least-square curve-fitting computer program is given in an Appendix.

CHAPTER II

EXPERIMENTAL APPARATUS AND PROCEDURES

The present experimental study was carried out in the UCLA Molecular-Beam Laboratory using the molecular-beam system shown schematically in Figure II-1. Since it has been described in detail elsewhere [1,2], only a brief description will be given here.

The satellite-speed (7000 m/sec) helium beams were generated using an arc-heated supersonic beam source developed by Young [3]. The incident beam was collimated by an orifice of 0.10-inch diameter placed between the collimation chamber and the detection chamber. The beam was characterized by a multi-disk velocity selector located in the collimation chamber.

A new detection system was constructed during the course of this study for facilitating measurements of the complete three-dimensional density and mean-energy distributions of satellite-speed helium atoms reflected from satellite surfaces. Cf. Figure II-2. This new system includes (1) a target positioning mechanism, (2) a detector rotating mechanism and (3) a mass spectrometer and/or a retarding-field energy analyzer. Descriptions of the first two mechanisms were given in the first report of this study (cf. ref. 1). The design and the operating procedure for the retarding-field energy analyzer will be given here.

The retarding-field energy analyzer is shown in Figures II-3 and II-4. An electron-impact ionizer, mounted 0.5-inch from the target surface on the entrance plate of the analyzer, was used to ionize a fraction of the beam species (also of the residual background). The retarding-field section of the analyzer is made of seven thin stainless-steel washer-shaped discs placed in a stainless-steel can. The inlet plate is followed by three

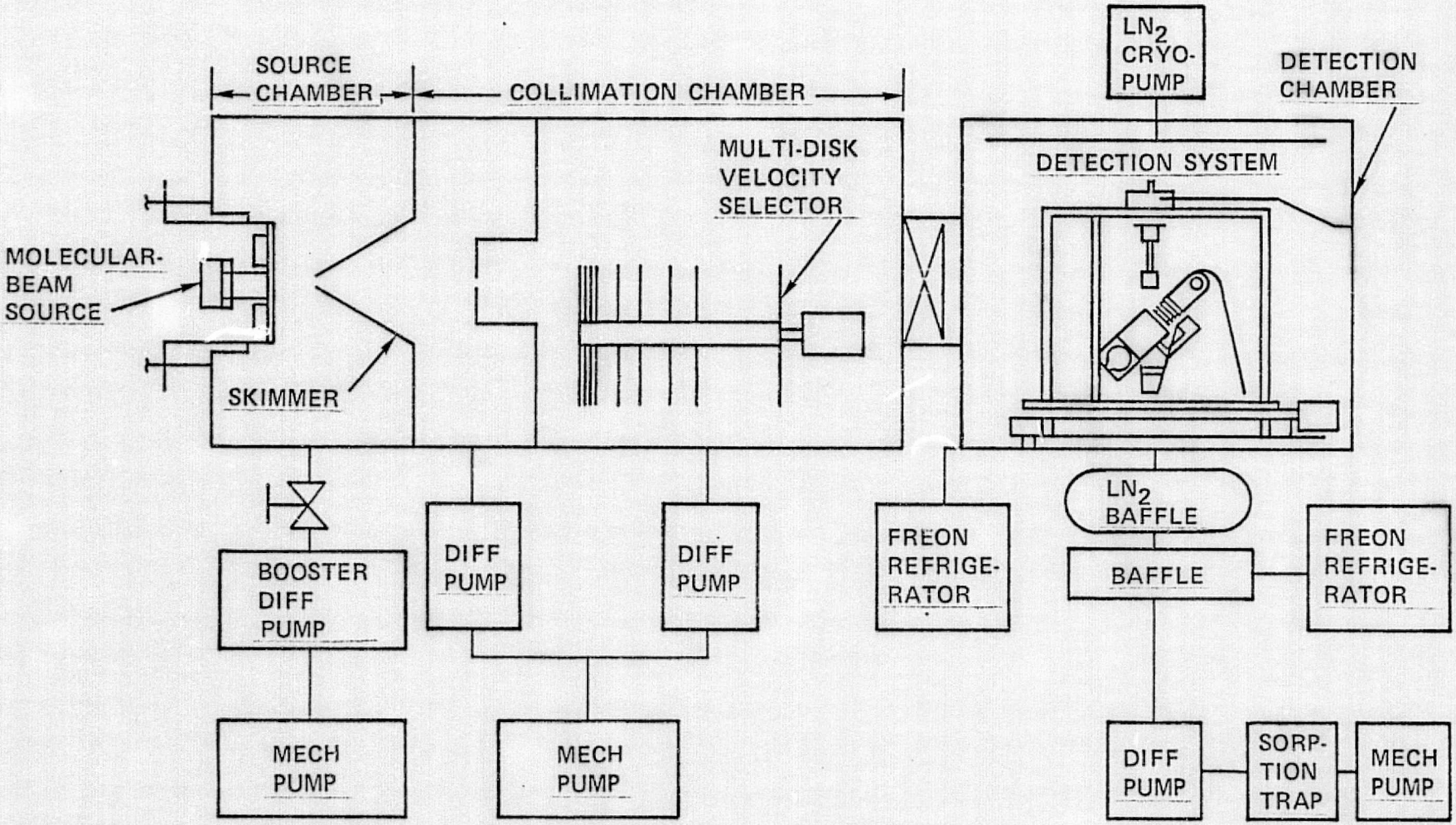

Figure II-1. Schematic Diagram of the Molecular Beam System.

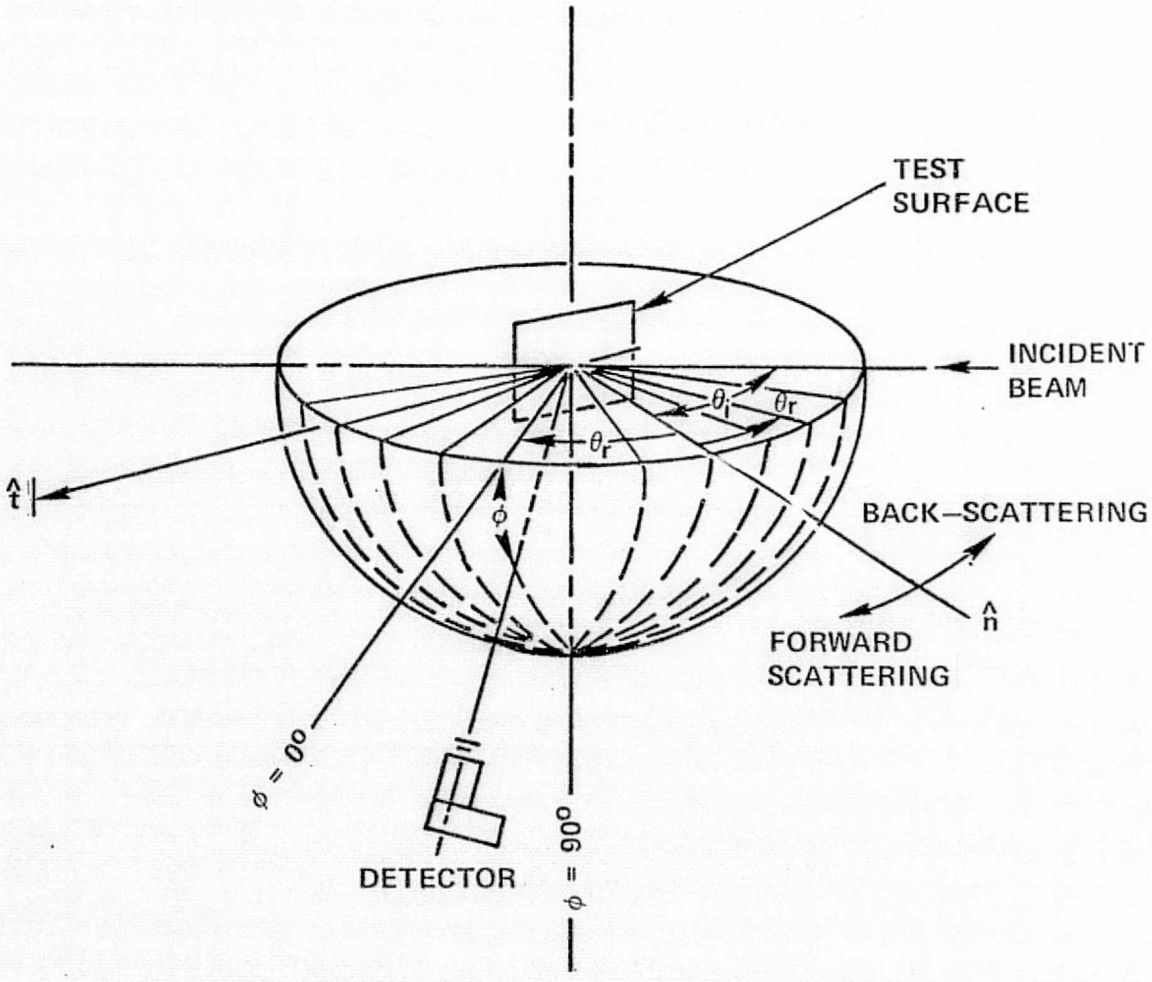

Figure II-2. Schematic Diagram of the Scattering System.

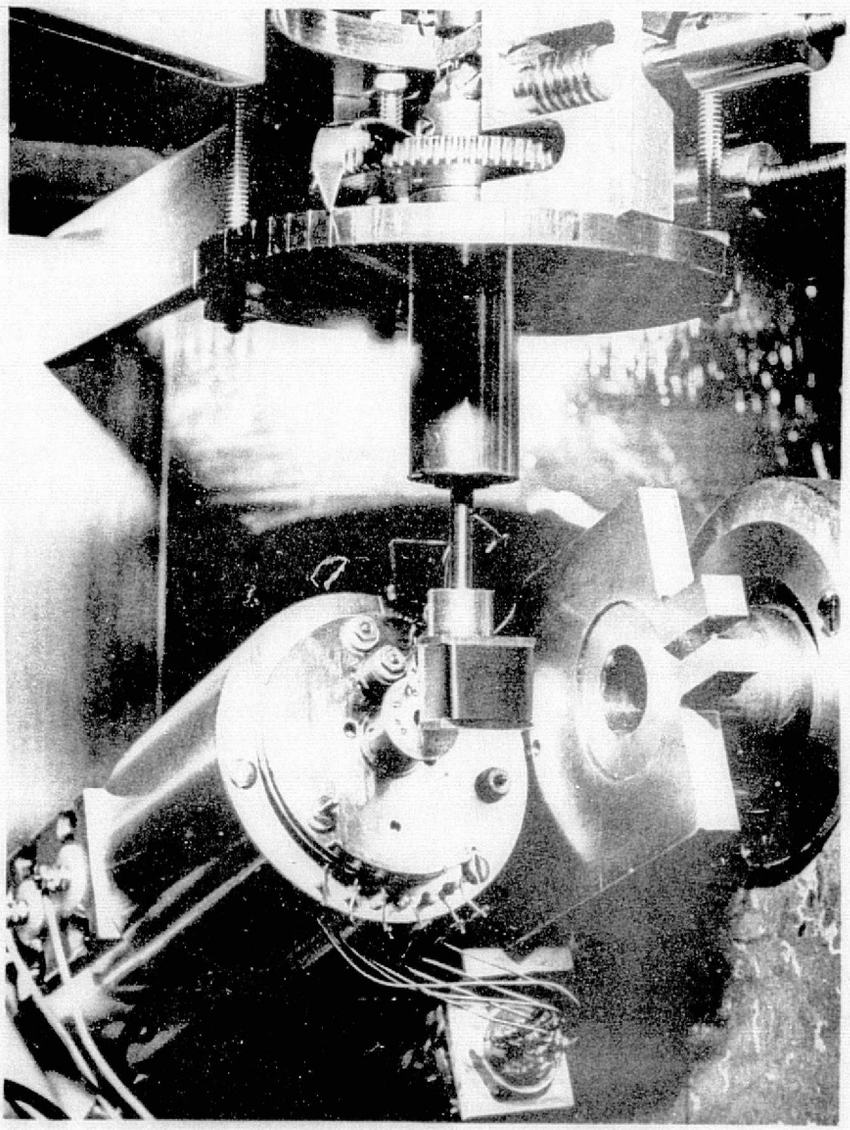

Figure II-3 Photograph of the Retarding-Field Energy Analyzer.

PLATE	APERTURE DIA (IN.)	POTENTIAL (V)
1	0.10	GROUND
2	0.25	$V_R - 175$
3	0.25	V_R
4	0.25 (MESH)	$V_R - 175$
5	0.25 (MESH)	V_R
6	0.25 (MESH)	$V_R - 175$
7	0.25	$V_R - 60$

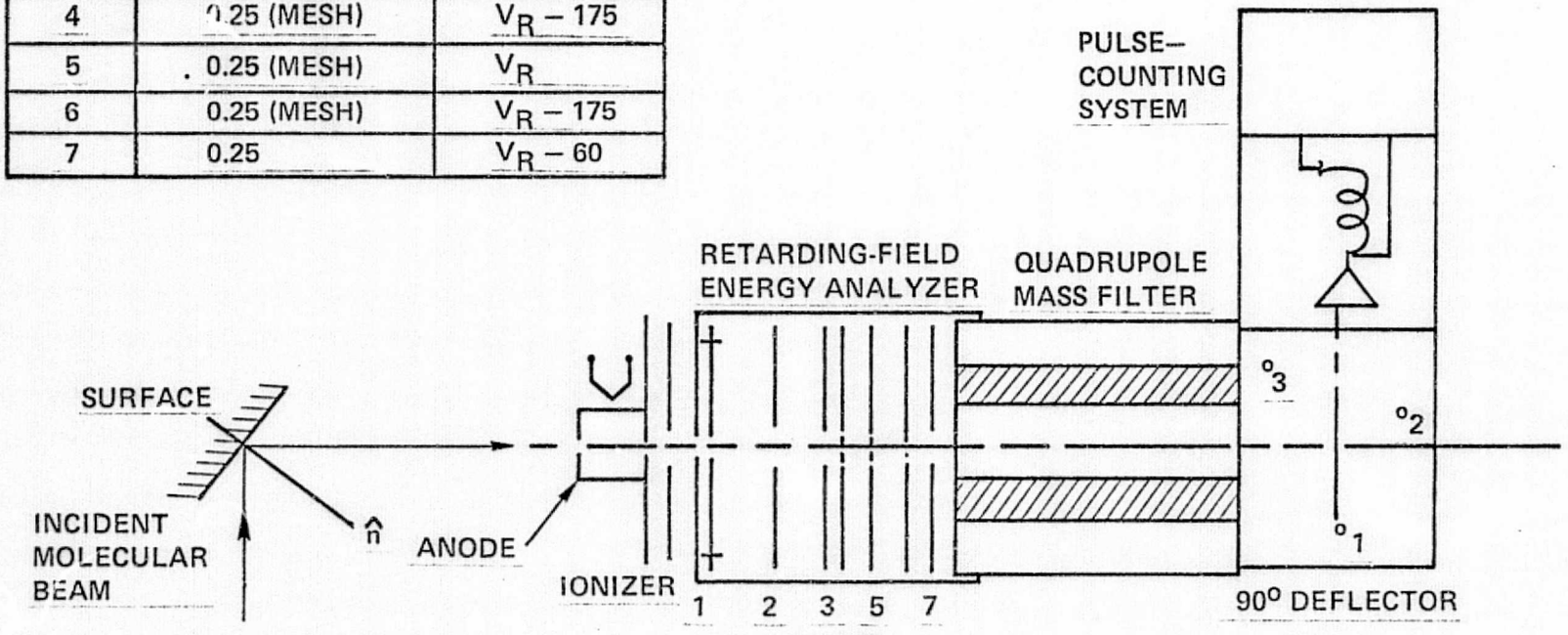

WIRE	POTENTIAL (VOLTS)
1	+50
2	+50
3	-500

Figure II-4. Schematic Diagram of the Retarding-Field Energy Analyzer.

focusing plates, a retarding plate and two more focusing plates. The potentials of all plates except that of the inlet plate are floated relative to the retarding potential so that ions of different energies will experience the same focusing effects within the analyzer. Thus undesirable effects of the energy-dependence of the transmission efficiency are minimized. Typical plate potentials also are given in Figure II-4.

The ions that have passed through the retarding-field region were filtered by a 2-inch quadrupole mass filter to eliminate the noise from the ionized background gases. The filtered ions were then detected by a pulse-counting particle detector. The energy spectrum of the reflected atoms at a given scattering position was obtained by measuring the reflected-beam density as a function of the retarding potential. The measured spectrum was processed by a NS513 signal averager and recorded on IBM cards. A block diagram of the electronic system is shown in Figure II-5.

Although the electron-impact ionization does not change the kinetic energy of a helium atom (since the translational energy transfer between the ionizing electron and the atom is negligible due to the large ratio of their masses), it was found that space-charge effects of ionizing electrons in the ionization region and/or surface-charge effects on the anode cage did introduce a systematic shift of the entire energy spectrum toward lower energies (i.e., the positive ions were produced in a region of negative potential with respect to ground). To reduce this shift, a small emission current ($\sim$ 50 μA) was used in the ionizer. Also, a positive potential (8 volts relative to ground) was applied to the anode cage in order to counter shift the energy spectrum toward higher energies. Then, since the potential of the ionization region was no longer at ground level, it was necessary to

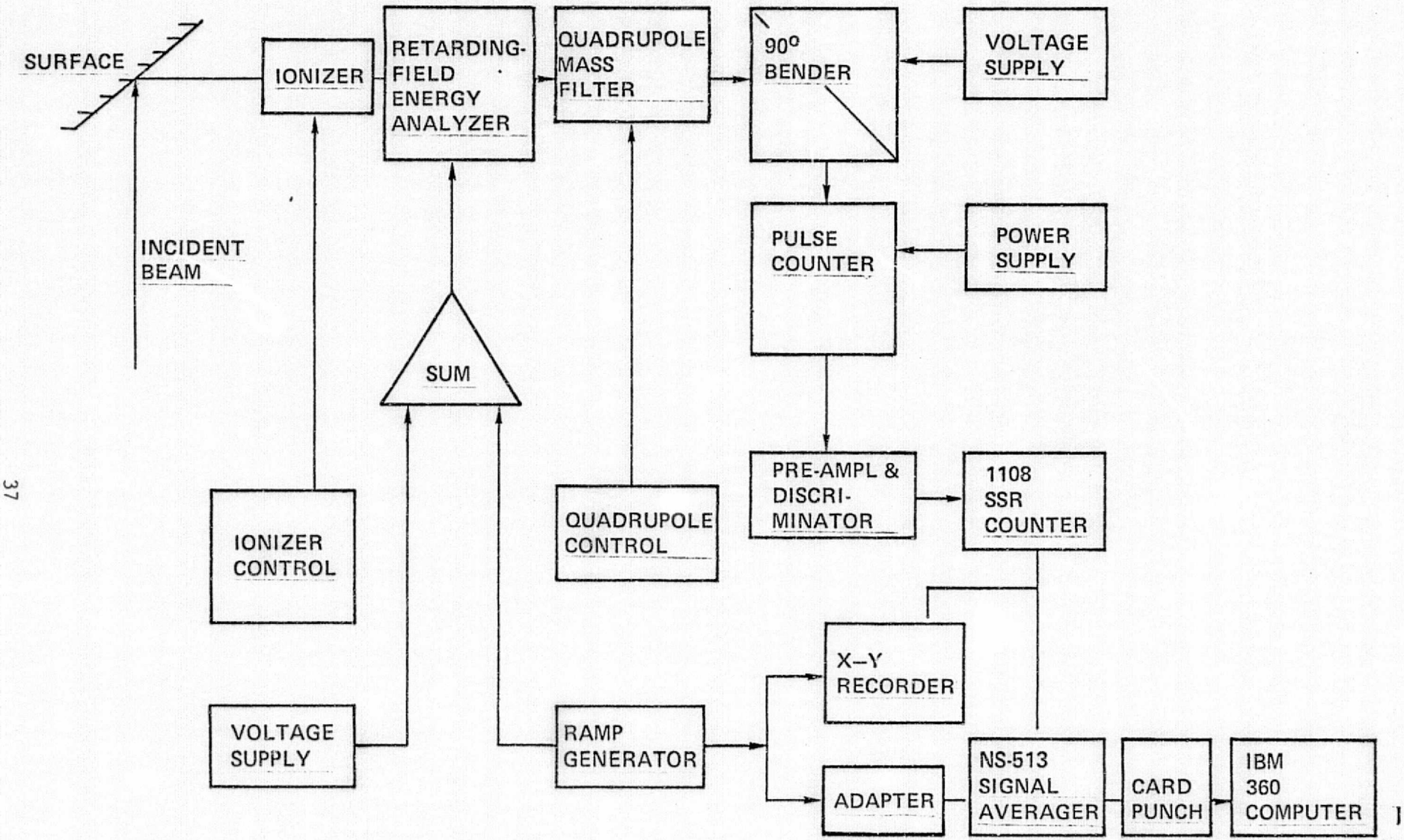

Figure II-5. Block Diagram of the Electronic System of the Retarding-Field Energy Analyzer.

ascertain independently a reference point in the energy spectrum. This reference point was provided by the thermal energy spectrum of the background gas, which has a mean thermal energy of 0.05 eV (i.e., the mean thermal energy at 296°K).

Since the background gas of the beam species also contributed to the measured spectrum, it was necessary to subtract this contribution in order to obtain the reflected-beam energy distributions. This subtraction was facilitated by measuring two spectra (one for the reflected beam plus background and one for the background alone) under the same operating conditions. Both spectra were then processed using a computer program; the reflected-beam energy spectrum was obtained by subtracting the background spectrum from the overall beam-energy spectrum. Both the background spectrum and the reflected-beam spectrum were least-square fitted using a high-order Chebyshev polynomial function. The differential energy distributions f(E) were obtained by simple differentiation of the fitted functions. The mean reflected-beam energy at a given scattering position was evaluated from

$$E_r(\theta_i,\theta_r,\phi) = \tilde{E}_r - \tilde{E}_{ref} + 0.05 \text{ (eV)} \qquad \text{(II-1)}$$

where

$$\tilde{E}(\theta_i,\theta_r,\phi) = \int f(E)\cdot E\cdot dE \Big/ \int f(E)\cdot dE \qquad \text{(II-2)}$$

and 0.05 eV is the thermal energy of the background gas at 296°K. The differential energy accommodation coefficient at a given scattering position was obtained using

$$[\text{A.C.}]_E(\theta_i,\theta_r,\phi) = \frac{E_i - E_r(\theta_i,\theta_r,\phi)}{E_i} \qquad \text{(II-3)}$$

where E_i is the incident-beam energy. The computer program and its input parameters for handling the described data reduction are given in the Appendix. The overall energy accommodation for a given incidence angle was then evaluated by

$$\overline{[A.C.]_E(\theta_i)} = \sum_{\theta_r} \sum_{\phi} n_i(\theta_i,\theta_r,\phi) \cdot [A.C.]_E(\theta_i,\theta_r,\phi) \qquad \text{(II-4)}$$

where $n_i(\theta_i,\theta_r,\phi)$ is the normalized spatial density-distribution function of reflected helium atoms.

As indicated, spatial distributions of satellite-speed helium beams scattered from four different satellite surfaces were obtained in the first phase of this study. Experimental procedures and results are included in report UCLA-ENG-7446 [1]. However, spatial distributions at some angles in the backscattering region were not measured at that time due to the constraint on the detector path as indicated in Figure II-6-(a). This problem was solved later by rotating the surface counterclockwise beyond the normal incidence angle while retaining the previous detector path as shown in Figure II-6-(b). Spatial and energy distributions were measured in the present study using these complementary configurations.

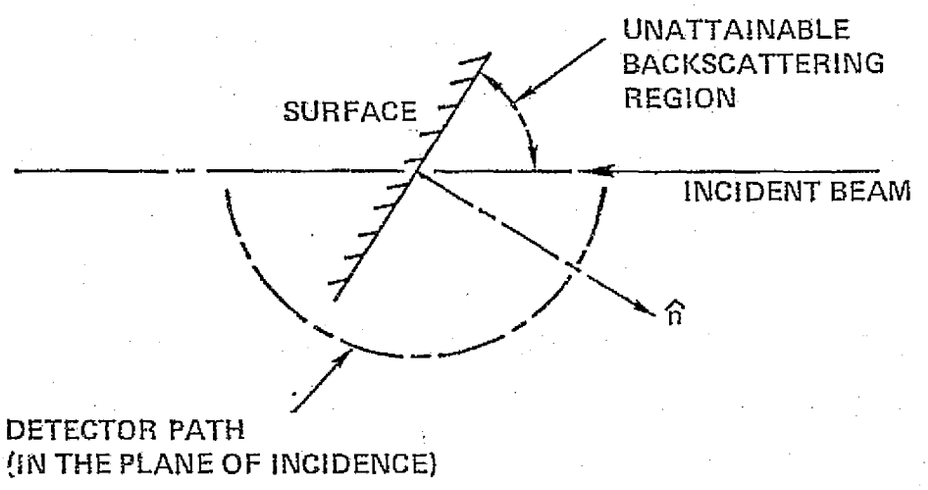

CONFIGURATION (a)

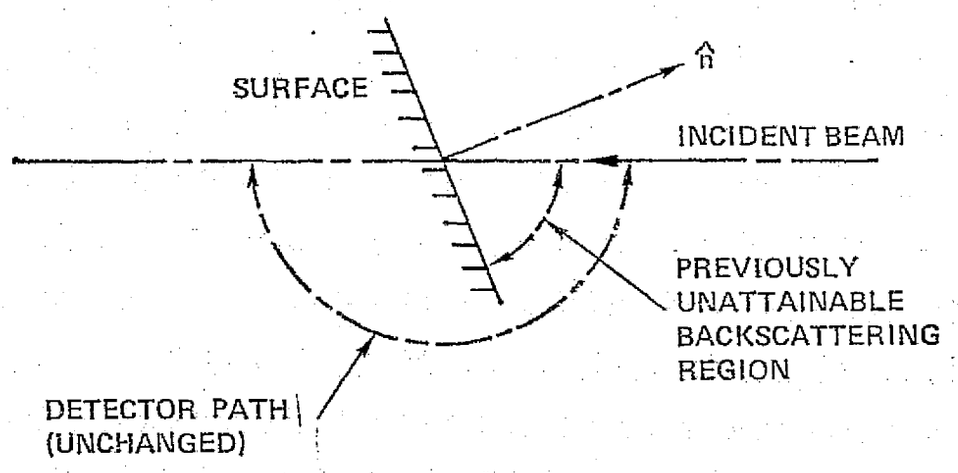

CONFIGURATION (b)

Figure II-6. Complementary Beam-Surface Configurations of the Scattering System.

CHAPTER III

RESULTS AND DISCUSSIONS

Spatial distributions of a satellite-speed (7000 m/sec) helium beam scattered from a cleaned 6061-T6 aluminum satellite surface for six different incidence angles (0°, 15°, 30°, 45°, 60° and 75° from the surface normal) are shown in Figures III-1 to III-6. The center of the polar diagram corresponds to the point of impingement. The incident beam impinges on the test surface (which coincides with the surface of the page) from the bottom of the diagram with the given incidence angle measured from the surface normal. The upper ($\theta_r > 0$) and lower ($\theta_r < 0$) halves of the diagram represent the forward-scattering and backward-scattering regions respectively. The dashed lines at constant value of θ_r indicate detector paths (i.e., from $\phi = 0°$ to $\phi = 90°$). ϕ denotes the out-of-plane scattering angle and $\phi = 0°$ represents the plane of incidence. These results show diffusive scattering patterns and exhibit trends similar to those previously reported [1]. As indicated before, the most interesting feature on these scattering patterns is the prominent backscattering of the incident helium atoms (i.e., a large fraction of the incident atoms are scattered back in the vicinity of the incident beam), particularly as the incidence angle increases toward the surface tangent (i.e., for large values of θ_i). This large fraction of backscattering could be due to the gross surface roughness and/or the relative lattice softness of the aluminum satellite surfaces. Smith [4] observed a large increase in backscattering intensity for increasing surface roughness in his computer simulation of gas molecule reflections from rough surfaces. This backscattering could result in relatively high drag coefficients for such satellite surfaces. The spatial-distribution

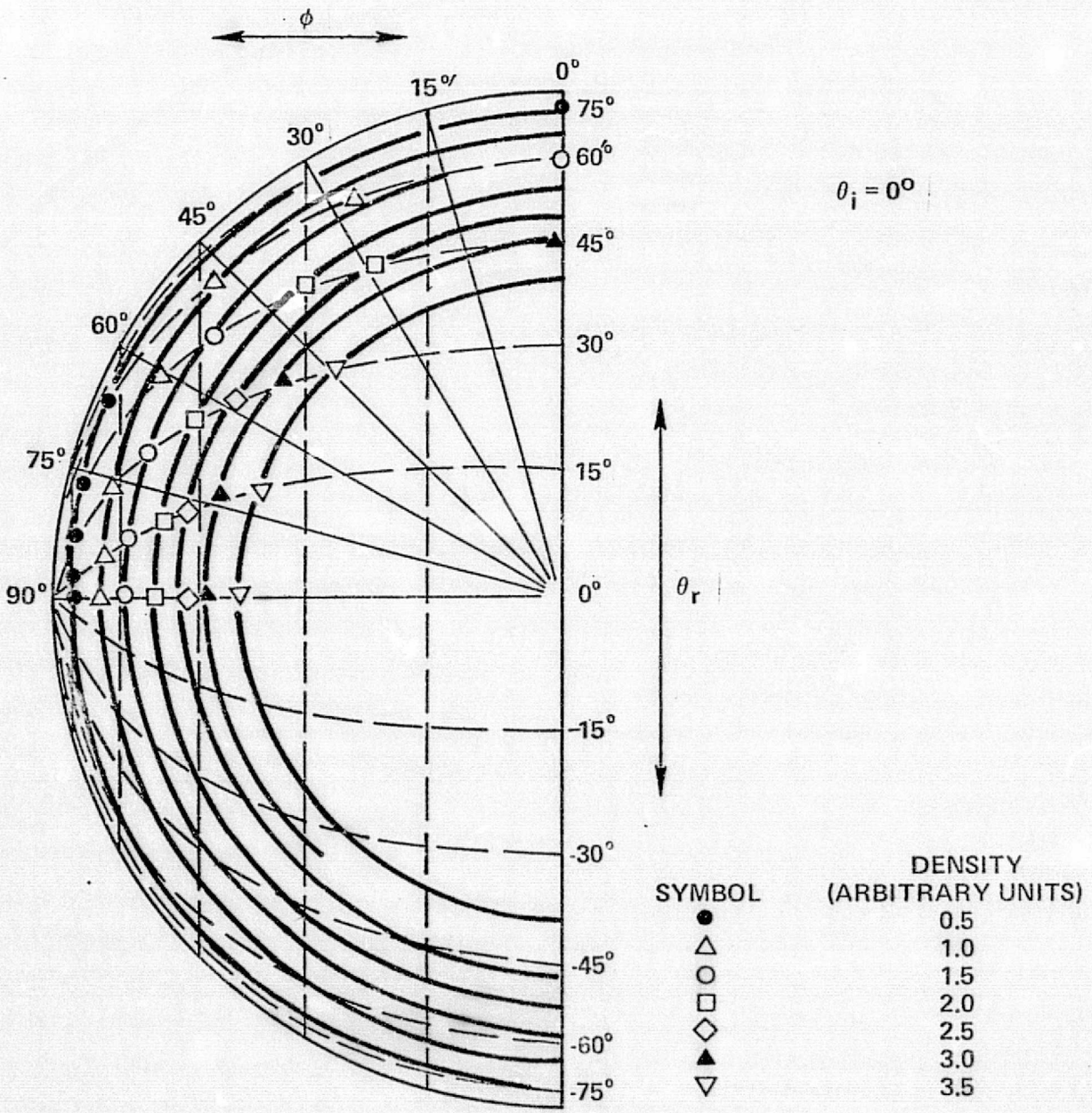

Figure III-1. Polar Plot of Scattered-Beam Density Distribution for 7000 m/sec Helium Beam Scattered from Cleaned 6061-T6 Aluminum Plate at 0^o Incidence Angle.

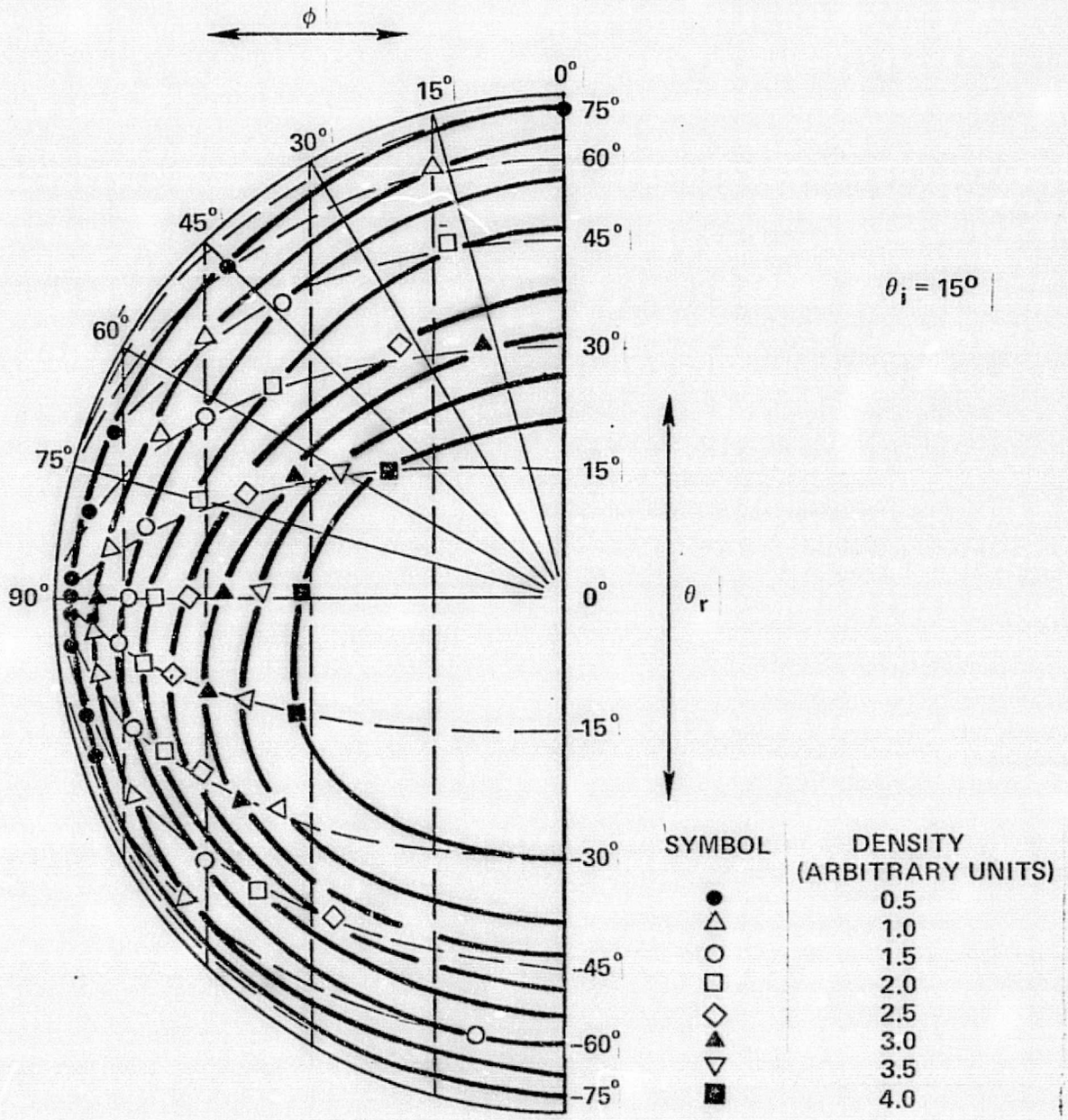

Figure III-2. Polar Plot of Scattered-Beam Density Distribution for 7000 m/sec Helium Beam Scattered from Cleaned 6061-T6 Aluminum Plate at 15° Incidence Angle.

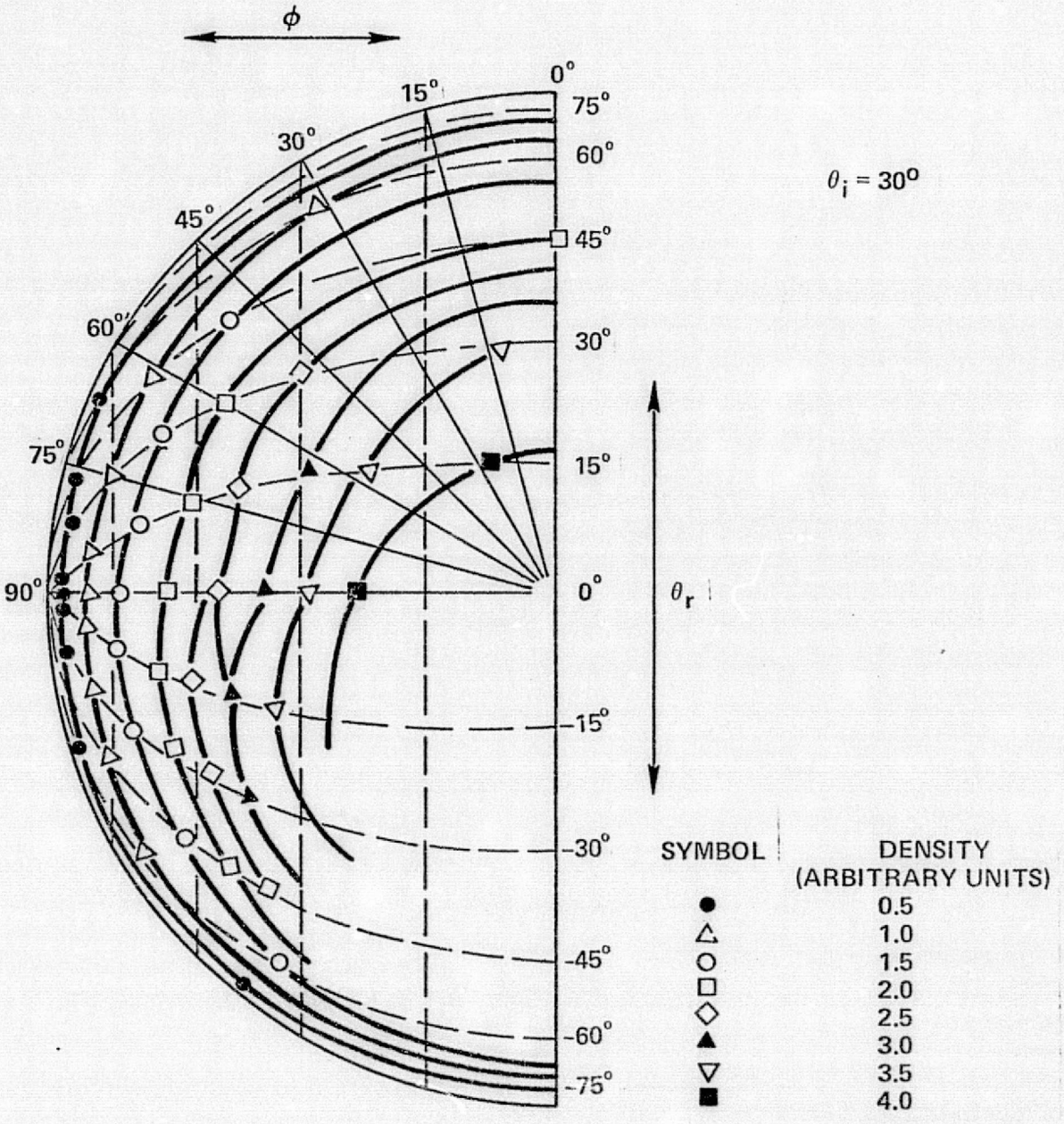

Figure III-3. Polar Plot of Scattered-Beam Density Distribution for 7000 m/sec Helium Beam Scattered from Cleaned 6061-T6 Aluminum Plate at 30^o Incidence Angle.

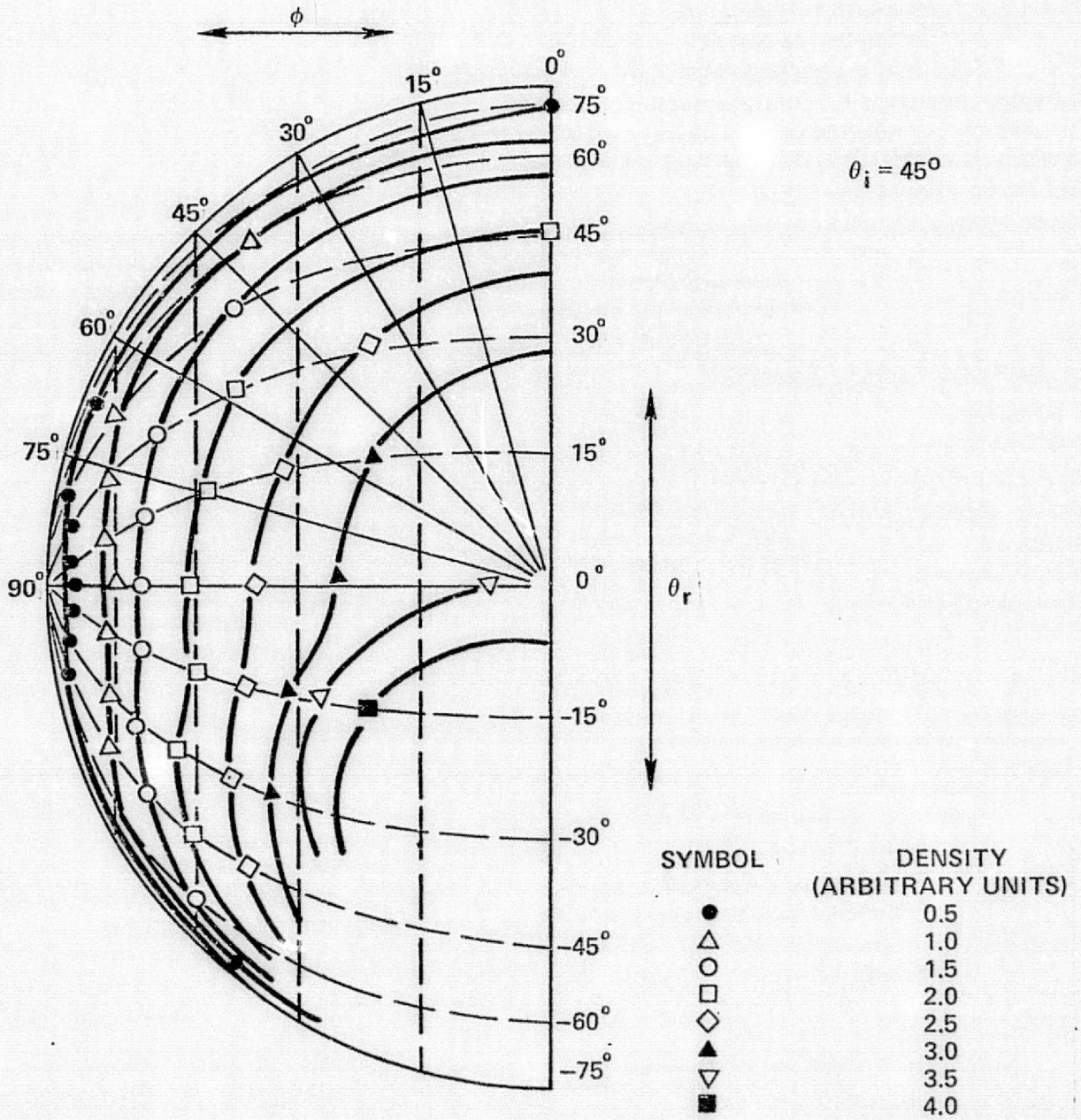

Figure III-4. Polar Plot of Scattered-Beam Density Distribution for 7000 m/sec Helium Beam Scattered from Cleaned 6061-T6 Aluminum Plate at 45° Incidence Angle.

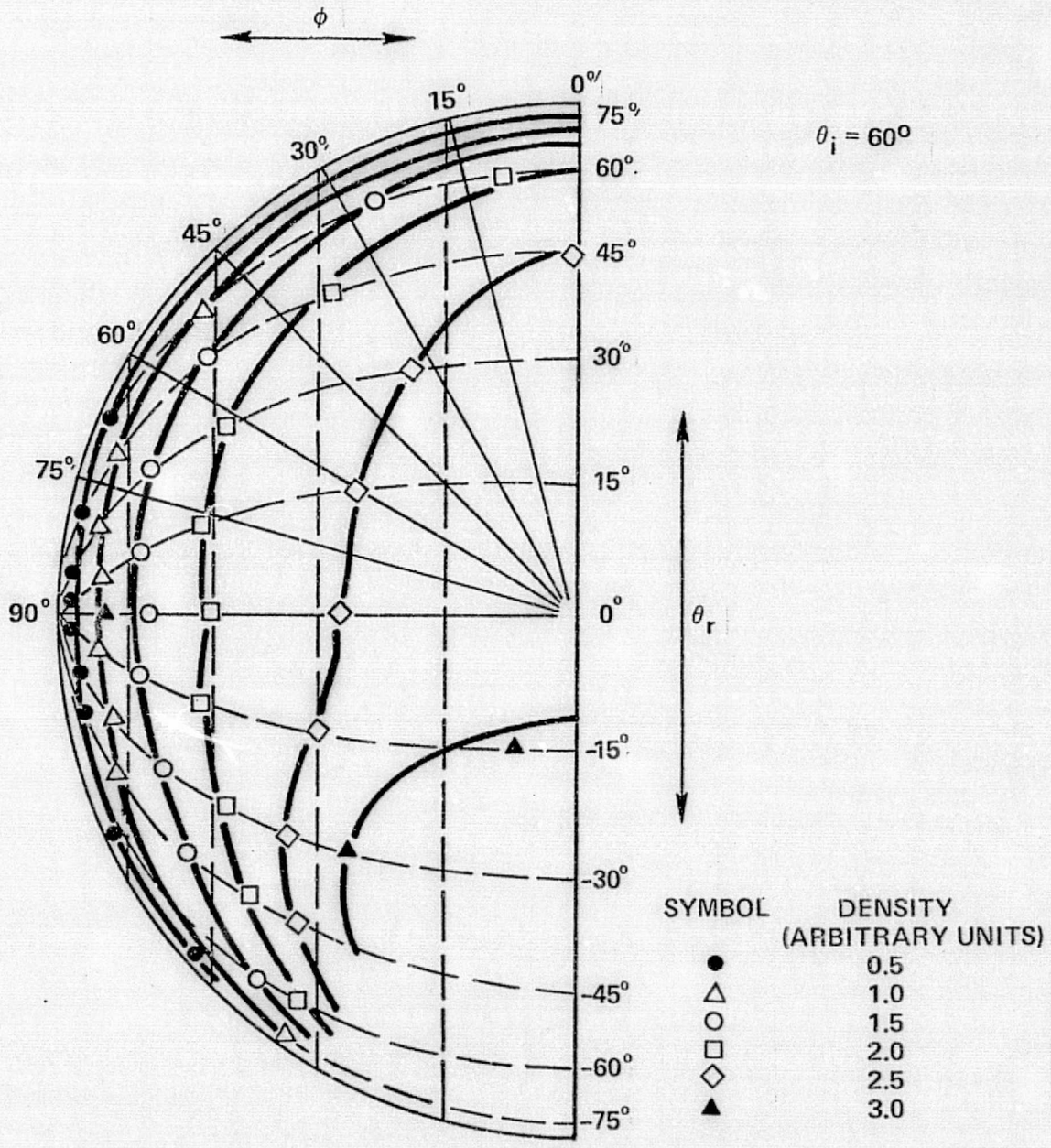

Figure III-5. Polar Plot of Scattered-Beam Density Distribution for 7000 m/sec Helium Beam Scattered from Cleaned 6061-T6 Aluminum Plate at 60^{o} Incidence Angle

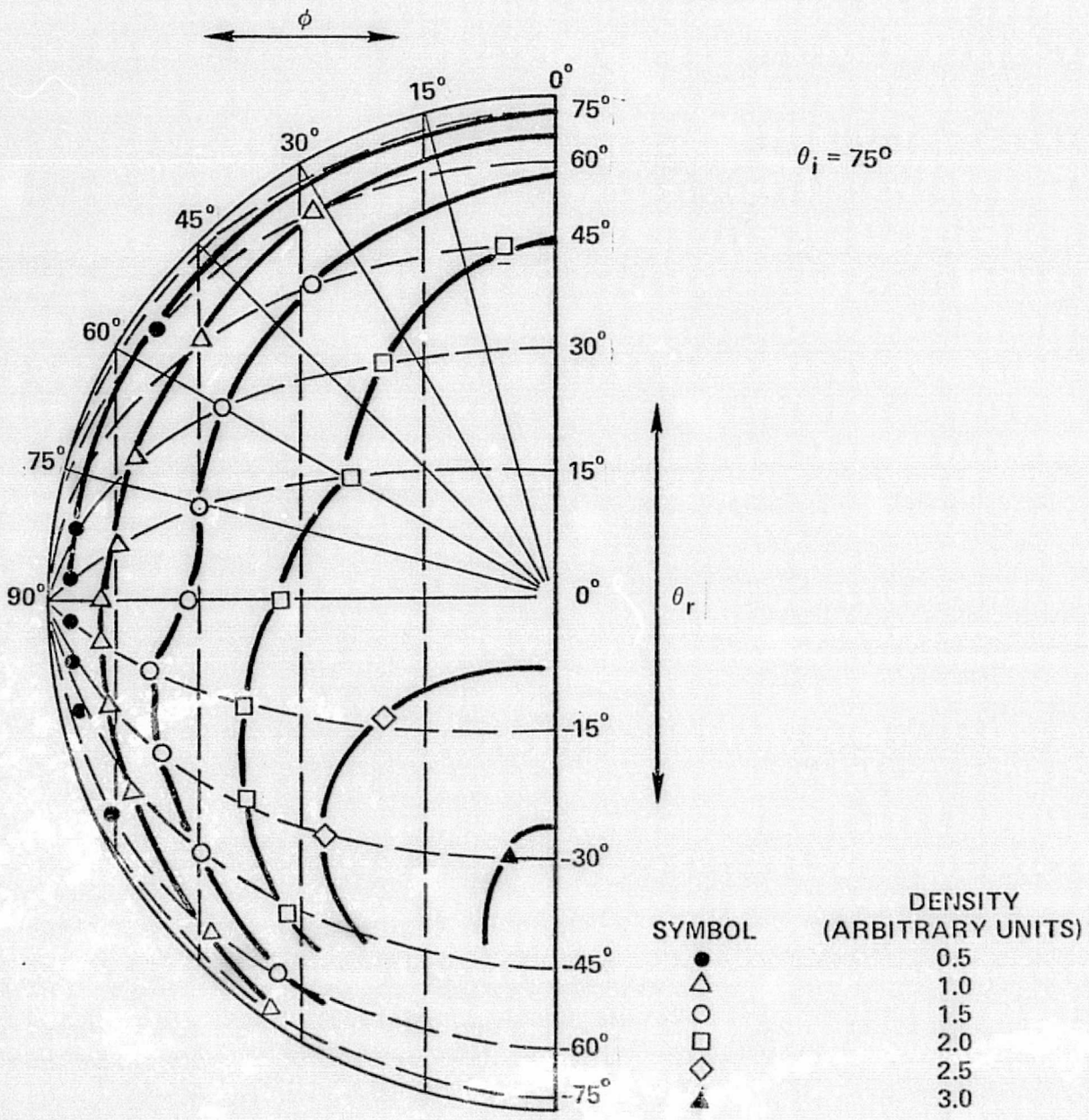

Figure III-6. Polar Plot of Scattered-Beam Density Distribution for 7000 m/sec Helium Beam Scattered from Cleaned 6061-T6 Aluminum Plate at 75° Incidence Angle.

measurements shown here and the energy-distribution measurements to be presented next provide the data required for estimating the overall energy accommodation for this beam-surface combination.

Measurements of energy distributions of satellite-speed helium atoms scattered from a cleaned 6061-T6 aluminum satellite surface were made for six different incidence angles (θ_i = 0°, 15°, 30°, 45°, 60° and 75° from the surface normal). For each incidence angle, distributions were measured at approximately sixty scattering positions. These scattering positions included eleven in-plane scattering angles (θ_r = ±75°, ±60°, ±45°, ±30°, ±15° and 0°) and six out-of-plane scattering angles (ϕ = 0°, 15°, 30°, 45°, 60° and 75°). Typical energy spectra obtained at a given scattering position are shown in Figures III-7 and III-8. Curve A of Figure III-7 represents the energy spectrum of a reflected helium beam superimposed on an energy spectrum of the background helium gas. Curve B of Figure III-7 represents the (thermal) energy of the background helium gas (mostly due to beam load). The reflected beam energy spectrum is then the difference of these two spectra (i.e., A-B). Figure III-8 shows the normalized energy spectra of the thermal background and the reflected helium atoms (Curves 3 and 1), their least-square fitted curves (Curves 4 and 2) and the corresponding differential energy distributions (Curves G and A) obtained using the computer program shown in Appendix A. The differential energy accommodation coefficient was obtained using Equations (II-1) and (II-3). Results for $(A.C.)_E(\theta_i,\theta_r,\phi)$ obtained at all possible scattering angles are given in Tables III-1 to III-6. Measurements were not possible within a solid angle around the incident beam (due to interference between the detector and the incident beam at these scattering positions) and for some glancing scattering angles (due to weak signal-to-noise ratios). These tables also include

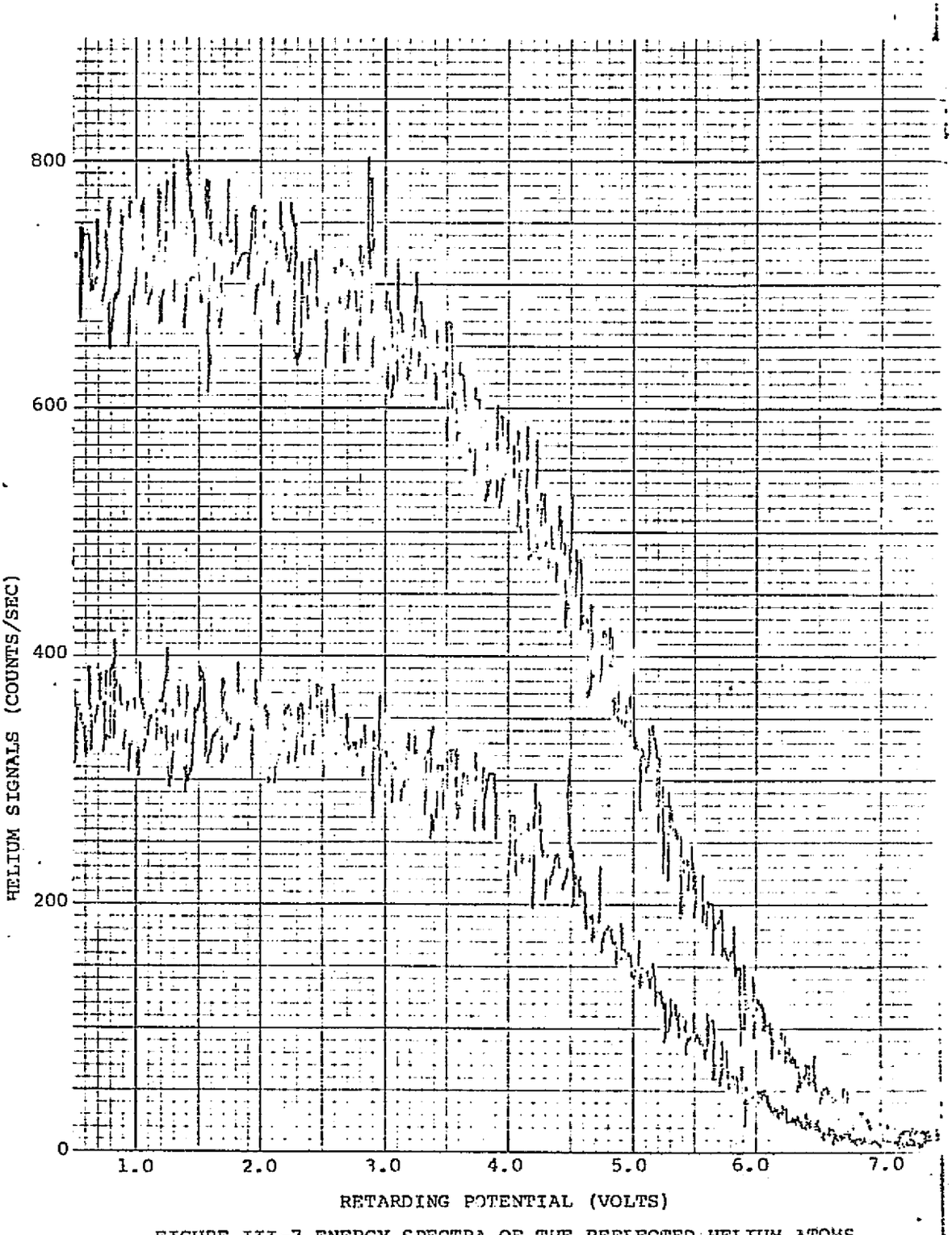

FIGURE III-7 ENERGY SPECTRA OF THE REFLECTED HELIUM ATOMS SUPERIMPOSED ON THE BACKGROUND (CURVE A) AND THE THERMAL BACKGROUND HELIUM GAS (CURVE B)

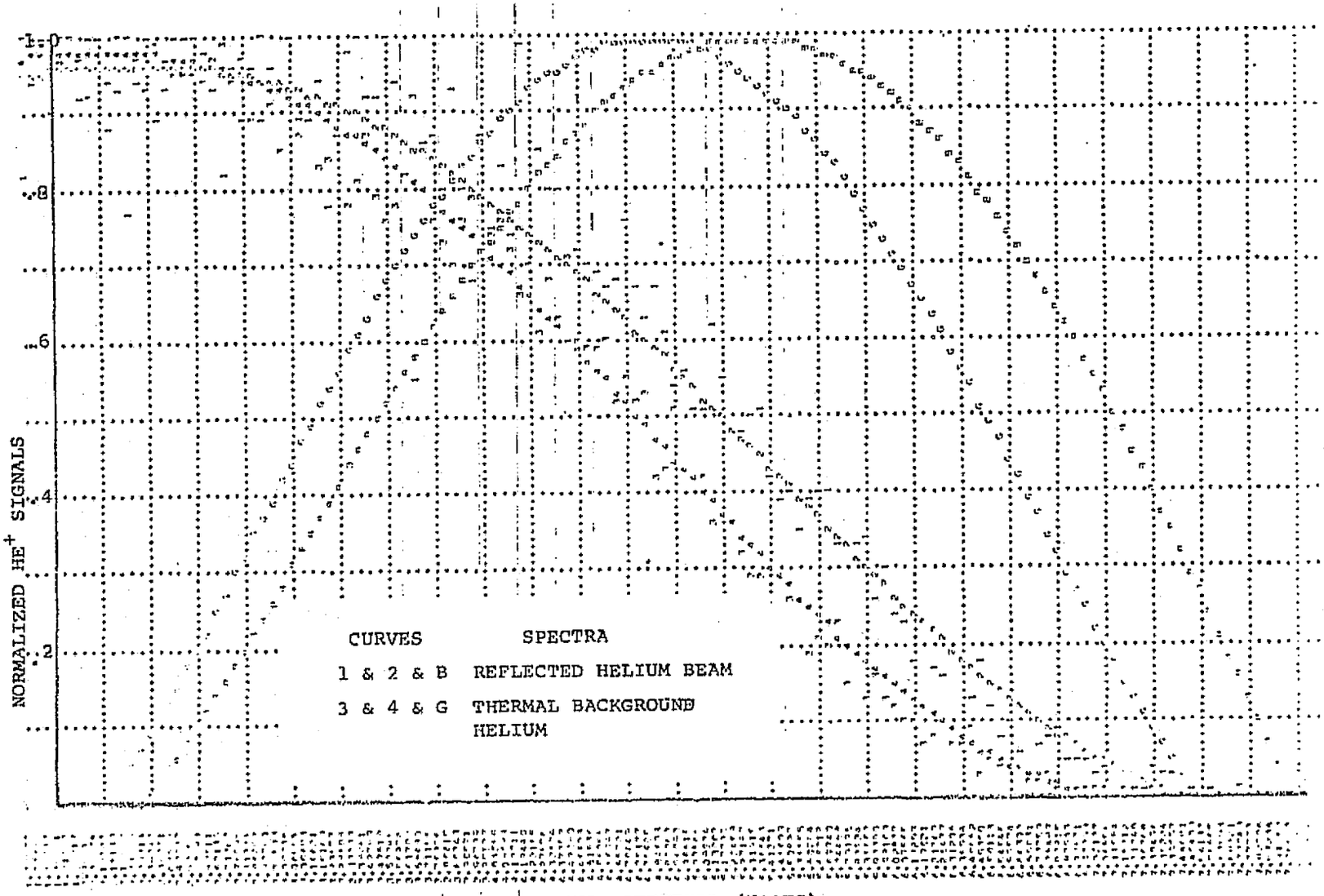

FIGURE III-8 LEAST-SQUARE FITTED ENERGY SPECTRA OF THE REFLECTED HELIUM ATOMS AND THE THERMAL BACKGROUND HELIUM GAS

Table III-1. The Differential Energy Accommodation Coefficients and the Normalized Spatial Density Distribution for 7000 m/sec Helium Beam Scattered From Cleaned 6061-T6 Aluminum Plate at 0^o Incidence Angle

ϕ \ θ_r	-75^o	-60^o	-45^o	-30^o	-15^o	$\pm o^o$	15^o	30^o	45^o	60^o	75^o
0^o	–	43[a] 3.3[b] 16[c]	56 6.6 12						56 6.6 12	43 3.3 16	–
15^o	–	55 3.1 14	52 5.9 11						52 5.9 11	55 3.1 14	–
30^o	–	63 2.4 15	54 4.4 13						54 4.4 13	63 2.4 15	–
45^o	–	–	55 3.3 21	58 4.6 14	55 5.9 11	54 6.4 11	55 5.9 11	58 4.6 14	55 3.3 21	–	–
60^o	–	–	–	43 2.4 14	45 3.1 17	46 3.3 17	45 3.1 17	43 2.4 14	–	–	–
75^o	–	–	–	–	–	–	–	–	–	–	–

NOTE:

(a) The Differential Accommodation Coefficient (%)
(b) The Normalized Spatial Density (%)
(c) Standard Deviaiton (%)

Table III-2. The Differential Energy Accommodation Coefficients and the Normalized Spatial Density Distribution for 7000 m/sec Helium Beam Scattered from Cleaned 6061-T6 Aluminum Plate at 15° Incidence Angle

ϕ \ θ_r	-75°	-60°	-45°	-30°	-15°	±0°	15°	30°	45°	60°	75°
0°	—	79[a] 3.4[b] 18[c]						48 7.1 14	46 4.8 12	38 3.0 20	—
15°	—	70 3.3 18						48 5.9 18	30 4.3 17	35 2.2 22	—
30°	—	77 2.8 18						47 5.0 18	45 3.4 20	—	—
45°	—	80 2.3 20	76 3.4 11	57 6.1 13	55 6.8 14	52 6.3 12	43 4.8 12	42 3.4 17	—	—	—
60°	—	77 1.6 25	83 2.3 16	61 4.6 20	62 4.8 19	60 4.6 13	55 3.9 19	—	—	—	—
75°	—	—	—	—	—	—	—	—	—	—	—

NOTE:

(a) The differential Accommodation Coefficient (%)
(b) The Normalized Spatial Density (%)
(c) Standard Deviation (%)

Table III-3. The Differential Energy Accommodation Coefficients and the Normalized Spatial Density Distribution for 7000 m/sec Helium Beam Scattered from Cleaned 6061-T6 Aluminum Plate at 30° Incidence Angle.

ϕ \ θ_r	-75°	-60°	-45°	-30°	-15°	±0°	15°	30°	45°	60°	75°
0°	58[a] 1.6[b] 27[c]						51 8.2 11	42 7.2 12	34 4.0 12	45 2.4 21	–
15°	41 1.6 26						48 7.6 11	38 6.2 13	40 3.8 18	50 2.2 21	–
30°	–						47 6.0 12	40 5.0 15	37 3.4 18	–	–
45°	–	67 2.2 19	60 3.0 13	59 4.8 9	57 5.2 11	60 5.0 19	49 4.0 21	40 3.4 20	–	–	–
60°	–	–	64 2.2 18	55 2.6 14	63 3.0 13	49 2.8 17	50 2.4 20	–	–	–	–
75°	–	–	–	–	–	–	–	–	–	–	–

NOTE:

(a) The Differential Accommodation Coefficient (%)
(b) The Normalized Spatial Density (%)
(c) Standard Deviation (%)

Table III-4. The Differential Energy Accommodation Coefficients and the Normalized Spatial Density Distribution for 7000 m/sec Helium Beam Scattered from Cleaned 6061-T6 Aluminum Plate at 45° Incidence Angle

ϕ \ θ_r	-75°	-60°	-45°	-30°	15°	±0°	15°	30°	45°	60°	75°
0°						49 6.7 10	-55 5.9 10	51 5.2 13	47 3.7 14	19 2.2 19	—
15°						42 6.3 11	41 5.8 10	37 4.9 21	34 3.5 14	25 1.9 20	—
30°						39 5.2 10	38 4.8 10	25 4.1 18	36 3.2 16	—	—
45°	55(a) 1.5(b) 28(c)	74 2.8 19	69 3.9 18	60 4.1 14	59 3.7 13	37 3.7 21	34 3.5 15	23 3.2 20	—	—	—
60°	—	67 1.5 28	56 2.0 28	60 2.2 18	58 2.2 13	21 2.2 30	—	—	—	—	—
75°	—	—	—	—	—	—	—	—	—	—	—

NOTE:

(a) The Differential Accommodation Coefficient (%)
(b) The Normalized Spatial Density (%)
(c) Standard Deviaition (%)

Table III-5. The Differential Energy Accomodation Coefficients and the Normalized Spatial Density Distribution for 7000 m/sec Helium Beam Scattered from Cleaned 6061-T6 Aluminum Plate at 60° Incidence Angle.

ϕ \ θ_r	-75°	-60°	-45°	-30°	-15°	±0°	15°	30°	45°	60°	75°
0°					62 6.2 12	58 5.8 13	63 5.5 15	66 5.2 15	51 5.0 18	—	—
15°					68 6.0 15	71 5.6 20	75 5.2 17	53 5.0 21	52 4.5 11	—	—
30°					70 5.0 17	74 4.9 36	73 4.8 32	56 4.5 11	—	—	—
45°	69(a) 2.0(b) 25(c)	65 2.6 22	61 3.4 19	67 3.8 14	66 4.0 20	74 4.0 36	—	—	—	—	—
60°	—	60 1.6 24	72 2.4 22	70 2.6 23	—	—	—	—	—	—	—
75°	—	—	—	—	—	—	—	—	—	—	—

NOTE:

(a) The Differential Accommodation Coefficient (%)
(b) The Normalized Spatial Density (%)
(c) Standard Deviation (%)

Table III-6. The Differential Energy Accommodation Coefficients and the Normalized Spatial Density Distribution for 7000 m/sec Helium Beam Scattered from Cleaned 6061-T6 Aluminum Plate at 75°Incidence Angle.

ϕ \ θ_r	-75°	-60°	-45°	-30°	-15°	±0°	15°	30°	45°	60°	75°
0°				72 7.0 11	66 6.1 8	64 5.4 13	51 5.0 20	50 4.8 16	45 4.5 30	—	—
15°				63 6.1 11	70 5.8 13	63 5.2 13	59 4.9 20	59 4.5 21	—	—	—
30°				80 5.4 13	60 5.0 13	53 4.5 14	—	—	—	—	—
45°	79[a] 1.9[b] 17	79 2.2 20	84 3.4 18	78 3.9 16	58 4.0 15	—	—	—	—	—	—
60°	66[c] 1.1 23	78 1.8 20	73 2.2 16	75 2.5 16	52 2.5 17	—	—	—	—	—	—
75°	—	—	—	—	—	—	—	—	—	—	—

NOTE:

(a) The Differential Accommodation Coefficient (%)
(b) The Normalized Spatial Density (%)
(c) Standard Deviation (%)

standard deviations (σ) of the reflected-beam energy-spectrum data from the least-square fitted curves and the normalized spatial-distribution function of the reflected helium atoms obtained from the measured spatial distributions shown in Figures III-1 to III-6. The overall energy accommodation coefficients at a given incidence angle was then evaluated using Equations (II-4) and the data given in these tables. The results are shown in Figure III-9.

The differential accommodations obtained show some fluctuations, due perhaps to the weak signal-to-noise ratio which results from the relatively diffusive scattering from the satellite-type aluminum surface. The results also indicate a weak dependence of accommodation on scattering angle, i.e., the $(A.C.)_E(\theta_i,\theta_r,\phi)$ decreases as the scattering direction shifts toward the surface tangent.

The overall accommodation coefficient is slightly higher for a glancing incident beam than for a normal incident beam. The value varies between 50% and 65% for this beam-surface combination.

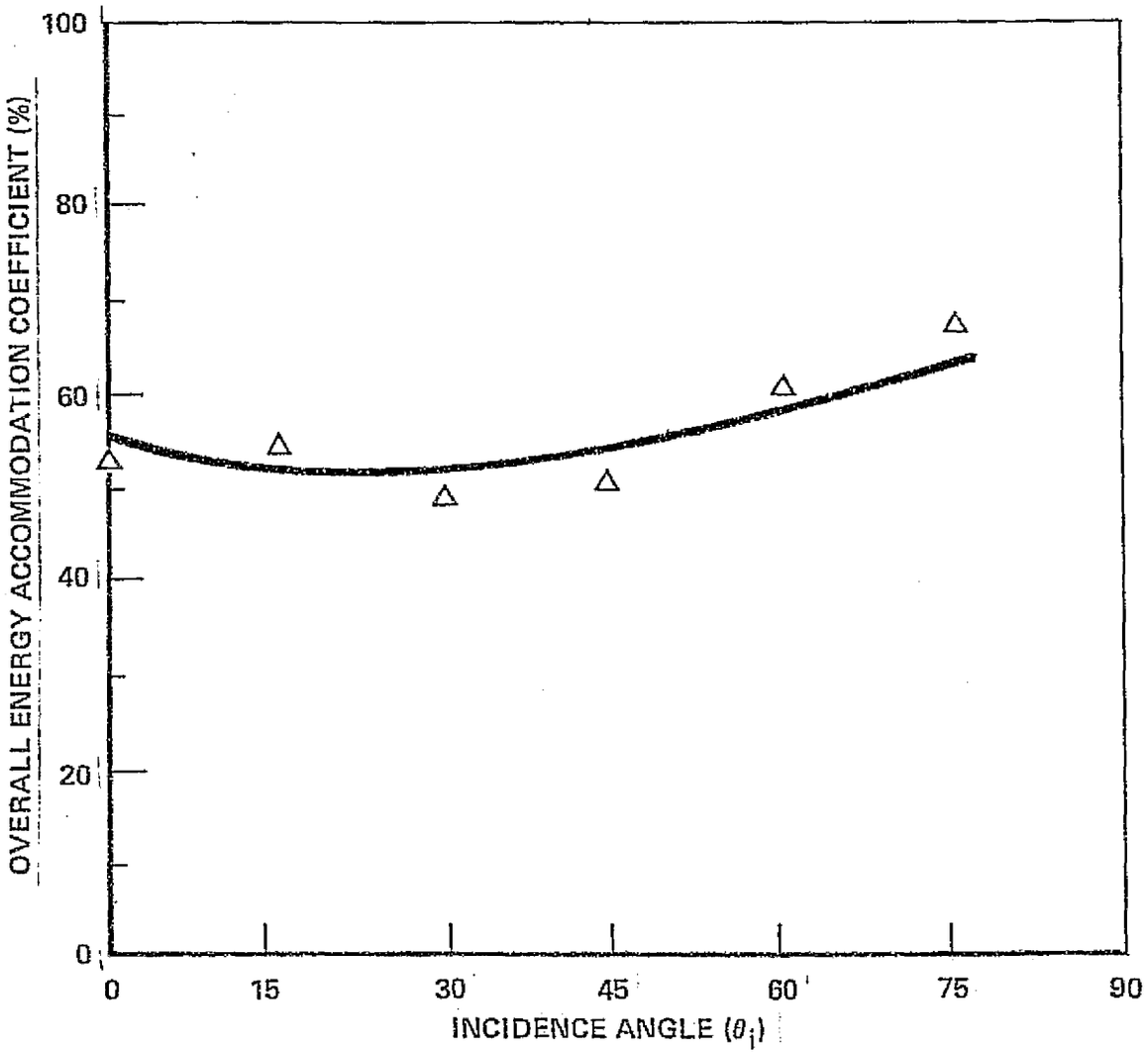

Figure III-9. Overall Energy Accommodation Coefficient of a Satellite-Speed Helium Beam (1.02 eV) Scattered From a Cleaned 6061-T6 Aluminum Surface as a Function of the Incidence Angle.

REFERENCES

1. Liu, S. M., W. E. Rodgers and E. L. Knuth, "Interactions of Satellite-Speed Helium Atoms with Satellite-Surfaces. I: Spatial Distributions of Reflected Helium Atoms," SEAS, UCLA, Report No. UCLA-ENG-7546, 1975.

2. Liu, S. M., "An Experimental Study of Interactions of Hyperthermal Atomic Beams with (111) Silver Surfaces and Adsorbed Molecules," SEAS, UCLA, Report No. UCLA-ENG-7510, 1975.

3. Young, W. S., "An Arc-Heated Ar-He Binary Supersonic Molecular Beam with Energies up to 21 eV," SEAS, UCLA, Report No. 69-39, 1969.

4. Smith, M. C., "Computer Study of Gas Molecule Reflections from Rough Surfaces," Rarefied Gas Dynamics (L. Trilling and H. Wachman, eds.), 2:1217-1220. New York: Academic Press, 1969.

APPENDIX

COMPUTER PROGRAM FOR LEAST-SQUARE FITTING

A. PROGRAM :

```
C
C     MAIN PROGRAM: INPUT; CALL; OUTPUT
C
      DIMENSION NC(512),
     1          Y(512),YBM(512),YBG(512),
     1          DYLS(512),
     1          EM2(2),SIGMA2(2),
     1          GF(251,101),GV(251)
      COMMON /AAA/X(512),YN(512),YLS(512),DY(512),N,EM,SIGMA,KM
      DATA BLANK/1H /,DOT/1H./
      DATA BM/1H1/,BML/1H2/,CBM/1HB/
      DATA BG/1H3/,BGL/1H4/,CBG/1HG/
    1 CONTINUE
      READ (5,800) NSET,KMON,KDAY,KYEAR,THETAI,THETAR,PHI
      IF (NSET.LT.1) GO TO 1000
      WRITE (6,900) KMON,KDAY,KYEAR,THETAI,THETAR,PHI
      IF (NSET.EQ.2) GO TO 5
      IF (NSET.GT.2) NSET=2
      READ (5,810) EI,M,NCV1,V1,NCV2,V2,NI,XLL,NF,XHL,
     1          INTI,INTF,KPG,KSTEP,NPW,NSTEP
      N=NF-NI+1
      DV=(V2-V1)/(NCV2-NCV1+1)
      VI=V1+DV*(NI-NCV1)
      VF=V1+DV*(NF-NCV1)
    5 CONTINUE
      IF (KPG.LT.1) GO TO 35
      DO 10 I=1,251
      GV(I)=0
      DO 10 J=1,101
      GF(I,J)=BLANK
   10 CONTINUE
      DO 20 I=1,251,5
      DO 20 J=1,101
      GF(I,J)=DOT
   20 CONTINUE
      DO 30 I=1,251
      DO 30 J=1,101,10
      GF(I,J)=DOT
   30 CONTINUE
   35 CONTINUE
      DO 40 I=1,32
      K=16*(I-1)
   40 READ (5,830) (YBG(K+J),J=1,16)
      IF (NSET.LT.2) GO TO 55
      DO 50 I=1,32
      K=16*(I-1)
      READ (5,830) (YBM(K+J),J=1,16)
      DO 50 J=1,16
   50 YBM(K+J)=YBM(K+J)-YBG(K+J)
   55 CONTINUE
      DO 500 KI=1,NSET
      DO 60 I=NI,NF
      K=I-NI+1
      NC(K)=I
```

```
      X(K)=VI+DV*(K-1)
      GO TO (61,62),KI
   61 Y(K)=YBG(I)
      GO TO 60
   62 Y(K)=YBM(I)
   60 CONTINUE
      SYMAX=0.0
      SYMIN=0.0
      DO 70 I=1,50
      SYMIN=SYMIN+Y(N-I)
   70 SYMAX=SYMAX+Y(I)
      YMIN=SYMIN/50.0
      YMAX=SYMAX/50.0
      DO 80 K=1,N
      YN(K)=(Y(K)-YMIN)/(YMAX-YMIN)
      IF (YN(K).GE.0.0) GO TO 75
      YN(K)=0.0
   75 IF (YN(K).LE.1.0) GO TO 80
      YN(K)=1.0
   80 CONTINUE
C
C     CALL LEAST-SQUARE CURVE FITTING
C
      CALL LSFCHV(N,XLL,XHL)
      GO TO (110,120),KI
  110 WRITE ( ,910)
      GO TO 130
  120 WRITE (6,915)
  130 CONTINUE
      IF (NPW.LT.1) GO TO 200
      WRITE (6,920)
      DO 190 K=1,N,NSTEP
      WRITE (6,930) NC(K),X(K),Y(K),YN(K),YLS(K),DY(K)
  190 CONTINUE
  200 CONTINUE
      EM=0.0
      SIGMA=0.0
      CALL EMEAN(INTI,INTF)
      EM2(KI)=EM
      CALL DEVIA
      SIGMA2(KI)=SIGMA
      SIGMAP=SIGMA*100.0
      WRITE (6,970) EM,SIGMAP
      IF (KPG.LT.1) GO TO 400
      KIN=1
      DO 290 K=1,N,KSTEP
      KIN=KIN+1
      GV(KIN)=X(K)
      JYN=100*ABS(YN(K))+1
      IF (JYN.LT.101) GO TO 291
      JYN=101
  291 CONTINUE
      IF (YLS(K).GE.0.0) GO TO 294
      JYLS=1
      GO TO 292
  294 CONTINUE
      JYLS=100*(ABS(YLS(K)))+1
      IF (JYLS.LT.101) GO TO 292
      JYLS=101
  292 CONTINUE
      JDY=100*ABS(DY(K))+1
      IF (JDY.LT.101) GO TO 293
      JDY=101
  293 CONTINUE
      GO TO (300,310),KI
  300 GF(KIN,JYN)=BG
      GF(KIN,JYLS)=BGL
      GF(KIN,JDY)=DBG
```

```
      GO TO 295
  310 GF(KIN,JYN)=BM
      GF(KIN,JYLS)=BML
      GF(KIN,JCY)=CBM
  295 CONTINUE
  290 CONTINUE
      IF (NSET.GT.1.AND.KI.LT.2) GO TO 400
      WRITE (6,940)
      GV(1)=GV(2)-(GV(3)-GV(2))
      DO 360 I=1,KIN
      WRITE (6,950) GV(I),(GF(I,J),J=1,101)
  360 CONTINUE
  400 CONTINUE
  500 CONTINUE
C
C     CALCULATE TRUE MEAN-BEAM ENERGY
C
      ACC=0.0
      IF (NSET.LT.2) GO TO 600
      ETRUE=EM2(2)-EM2(1)+0.05
      ACC=(EI-ETRUE)/EI*100
  600 CONTINUE
      WRITE (6,975)
      WRITE (6,980) ETRUE,ACC
      WRITE (6,975)
      GO TO 1
  800 FORMAT (4I10,3F10.3)
  810 FORMAT (F5.2,I5,4(I3,F7.2),6I5)
  830 FORMAT (16F5.0)
  910 FORMAT (12X,23H** SET 1: BACKGROUND **/)
  900 FORMAT (///2X,7HDATE : ,I2,1H/,I2,1H/,I2,5X,
     1       26HANGLES(THETAI/THETAR/PHI):,F6.2,1H/,F6.2,1H/,F6.2/)
  915 FORMAT (12X,17H** SET 2: BEAM **/)
  920 FORMAT (3X,7HCH. NO.,12X,3HV-R,11X,5HI-SIG,13X,5HI-NOR,
     1       10X,7HLSI-NOR,8X,9HD(LSI)/DV)
  930 FORMAT (5X,I5,10X,F6.3,10X,F6.1,3(10X,F7.4))
  940 FORMAT (//8X,3HV/R,10X,7H1:I(BM),3X,9H2:LSI(BM),3X,
     1        16HB:D(LSI)/DV-(BM),3X,7H3:I(BG),3X,9H4:LSI(BG),
     2        3X,16HD(LSI)/DV-(BG)//)
  950 FORMAT (2X,F10.5,3X,101A1)
  970 FORMAT (/5X,12HMEAN-ENERGY:,F7.4,3H EV,10X,19HSTANDARD DEVIATION:,
     1       2X,F5.2,1H%/)
  975 FORMAT(//10X,80H**********************************************************
     1**********//)
  980 FORMAT(/10X,22HTRUE MEAN-BEAM ENERGY:,2X,F7.4,3X,2HEV,10X,
     1       26HACCOMMODATION COEFFICIENT=,F7.4,1H%/)
C
 1000 CONTINUE
      STOP
      END



C
      SUBROUTINE LSFCHV(M,XLL,XHL)
C   M >= 2
      DIMENSION T(10),DT(10)
      COMMON /AAA/X(512),Y(512),YLS(512),DY(512),N,EM,SIGMA,KM
      COMMON /SIM/A(100),R(10)
      M1=M+1
C     INITIALIZATION
      DO 2 I=1,M1
    2 R(I)=0.0
      M2=M1*M1
      DO 4 I=1,M2
    4 A(I)=0.0
      XD=2.0/(X(N)-X(1))
      XO=(X(N)+X(1))/(X(N)-X(1))
C     CALCULATE CHEBYSHEV FUNCTION AT TX
      T(1)=1.0
      DO 30 K=1,N
      TX=XD*X(K)-XO
      T(2)=TX
      DO 10 I=3,M1
   10 T(I)=2.0*TX*T(I-1)-T(I-2)
```

```
      DO 20 I=1,M1
      R(I)=R(I)+T(I)*Y(K)
      DO 20 J=1,M1
      IJ=(I-1)*M1+J
   20 A(IJ)=A(IJ)+T(I)*T(J)
   30 CONTINUE
      EPS=1.0E-60
      IER=0
      CALL SIMQ(M1,1,EPS,IER)
C     CALCULATE CHEBYSHEV POLYNOMIAL AT TX USING R(I)
C     CALCULATE DY FORM CHEBYSHEV POLYNOMIAL
      DT(1)=0.0
      DT(2)=1.0
      DO 80 K=1,N
      YLSK=0.0
      DYK=0.0
      TX=XD*X(K)-XO
      T(2)=TX
      DO 35 I=3,M1
   35 T(I)=2.0*TX*T(I-1)-T(I-2)
      DO 40 I=1,M1
   40 YLSK=YLSK+T(I)*R(I)
   50 YLS(K)=YLSK
      DO 60 I=3,M1
   60 DT(I)=2.0*(T(I-1)+TX*DT(I-1))-DT(I-2)
      DO 70 I=2,M1
   70 DYK=DYK+R(I)*DT(I)
      IF (DYK.LE.0.0) GO TO 80
      DYK=0.0000001
   80 DY(K)=DYK
      DYM=0.0
      DO 250 K=1,N
      IF (X(K).LT.XLL.OR.X(K).GT.XHL) GO TO 250
  240 IF (DY(K).GT.0.0) GO TO 250
      IF (DYM.GT.ABS(DY(K))) GO TO 250
      DYM=ABS(DY(K))
      KM=K
  250 CONTINUE
      KRS=0
      K=0
  280 K=K+1
      KR=KM-K+1
      IF (KR.LT.1) GO TO 290
      IF (KRS.GT.1) GO TO 285
      DY(KR)=DY(KR)/DYM
      IF (DY(KR).LT.0.0) GO TO 280
      KRS=2
  285 DY(KR)=-0.0000001/DYM
      GO TO 280
  290 K=0
      KFS=0
  292 K=K+1
      KF=KM+K
      IF (KF.GT.N) GO TO 300
      IF (KFS.GT.1) GO TO 294
      DY(KF)=DY(KF)/DYM
      IF (DY(KF).LT.0.0) GO TO 292
      KFS=2
  294 DY(KF)=-0.0000001/DYM
      GO TO 292
  300 CONTINUE
      RETURN
      END
```

```
      SUBROUTINE DEVIA
      COMMON /AAA/X(512),YN(512),YLS(512),DY(512),N,EM,SIGMA,KM
      SY=0.0
      SQ=0.0
      DO 100 K=1,N
      SY=SY+YN(K)
      DIFF=YN(K)-YLS(K)
  100 SQ=SQ+(ABS(DIFF))**2.0
      SIGMA=(SQ/N)**(0.5)/(SY/N)
      RETURN
      END


      SUBROUTINE EMEAN(INTI,INTF)
      COMMON /AAA/X(512),YN(512),YLS(512),DY(512),N,EM,SIGMA,KM
      SYDE=0.0
      SYEDE=0.0
      KR=0
  280 CONTINUE
      KR=KR+1
      K=KM-KR+1
      IF (K.LT.2.OR.KR.GT.INTI) GO TO 290
      SYDE=SYDE+0.5*(DY(K)+DY(K-1))*(X(K)-X(K-1))
      SYEDE=SYEDE+0.5*(DY(K)+DY(K-1))*0.5*(X(K)+X(K-1))*(X(K)-X(K-1))
      GO TO 280
  290 CONTINUE
      KF=0
  300 CONTINUE
      KF=KF+1
      K=KM+KF
      IF (K.GT.N.OR.KF.GT.INTF) GO TO 310
      SYDE=SYDE+0.5*(DY(K)+DY(K-1))*(X(K)-X(K-1))
      SYEDE=SYEDE+0.5*(DY(K)+DY(K-1))*0.5*(X(K)+X(K-1))*(X(K)-X(K-1))
      GO TO 300
  310 CONTINUE
      EM=SYEDE/SYDE
      RETURN
      END


C
      SUBROUTINE SIMQ(M,N,EPS,IER)
C     DIMENSION A(MM),R(NM)
      COMMON /SIM/A(100),R(10)
      NM=N*M
      MM=M*M
      IF(M) 23,23,1
    1 IER=0
      PIV=0.
      DO 3 L=1,MM
      TB=ABS(A(L))
      IF (TB-PIV) 3,3,2
    2 PIV=TB
      I=L
    3 CONTINUE
      TOL=EPS*PIV
      LST=1
      DO 17 K=1,M
      IF (PIV) 23,23,4
    4 IF (IER) 7,5,7
    5 IF (PIV-TOL) 6,6,7
    6 IER=K-1
    7 PIVI=1./A(I)
      J=(I-1)/M
      I=I-J*M-K
      J=J+1-K
```

```
      DO 8 L=K,NM,M
      LL=L+I
      TB=PIVI*R(LL)
      R(LL)=R(L)
    8 R(L)=TB
      IF (K-M) 9,13,18
    9 LEND=LST+M-K
      IF(J) 12,12,10
   10 II=J*M
      DO 11 L=LST,LEND
      TB=A(L)
      LL=L+II
      A(L)=A(LL)
   11 A(LL)=TB
   12 DO 13 L=LST,NM,M
      LL=L+I
      TB=PIVI*A(LL)
      A(LL)=A(L)
   13 A(L)=TB
      A(LST)=J
      PIV=0.0
      LST=LST+1
      J=0
      DO 16 II=LST,LEND
      PIVI=-A(II)
      IST=II+M
      J=J+1
      DO 15 L=IST,NM,M
      LL=L-J
      A(L)=A(L)+PIVI*A(LL)
      TB=ABS(A(L))
      IF (TB-PIV) 15,15,14
   14 PIV=TB
      I=L
   15 CONTINUE
      DO 16 L=K,NM,M
      LL=L+J
   16 R(LL)=R(LL)+PIVI*R(L)
   17 LST=LST+M
   18 IF (M-1) 23,22,19
   19 IST=NM+M
      LST=M+1
      DO 21 I=2,M
      II=LST-I
      IST=IST-LST
      L=IST-M
      L=A(L)+.5
      DO 21 J=II,NM,M
      TB=R(J)
      LL=J
      DO 20 K=IST,NM,M
      LL=LL+1
   20 TB=TB-A(K)*R(LL)
      K=J+L
      R(J)=R(K)
   21 R(K)=TB
   22 RETURN
   23 IER=-1
      RETURN
      END
```

B. RUN PARAMETER

DATA CARD

#1 READ (NSET, KMON, KDAY, KYEAR, THETAI, THETAR, PHI)

NSET (I10)

> 2: Run with calibration parameters

(or=1) (Data Card #2)

= 2: Run without re-calibrations

KMON, KDAY, KYEAR (3I10)

MONTH/DAY/YEAR

THETAI, THETAR, PHI (3F10.3)

Angular parameters (θ_i,θ_r,ϕ)

#2 (Req. if NSET > 2 or = 1) READ (EI, M, NCVI, VI, NCV2, V2, NI, XLL, NF, XHL, INTI, INTF, KPG, KSTEP, NPW, NSTEP)

EI (F5.2): Incidemt-beam energy

M(I5): Order of the lest-square fitting program

NCVI (I3)
VI (F7.2)
NCV2 (I3)
V2 (F7.2)
} Calibration of x-coordinate

NI (I3)
XLL (F7.2)
NF (I3)
XHL (F7.2)
} Operational limits

INTI (I5)
INTF (I5)
} Integration Limits

KPG (I5): Graphical Index

> 1 : with graphical output

< 1 : without graphical output

KSTEP (I5): Step-size for graphical output

NPW (I5): Output index

> 1 : with detail output

< 1 : without detail output

NSTEP (I5): Step-size for detail output

#3-#28 DATA SET: For thermal background gas

#29-#54 DATA SET: For reflected beam

ENDCARD: (Blank)